

Cite this: *Energy Environ. Sci.*, 2012, **5**, 6022

www.rsc.org/ees

PERSPECTIVE

Photovoltaic efficiency limits and material disorder

Pabitra K. Nayak,^a Germà Garcia-Belmonte,^b Antoine Kahn,^c Juan Bisquert^{*b} and David Cahen^{*a}

Received 15th November 2011, Accepted 6th January 2012

DOI: 10.1039/c2ee03178g

Solar cells based on crystalline semiconductors such as Si and GaAs provide nowadays the highest performance, but photovoltaic (PV) cells based on less pure materials, such as poly- or nano-crystalline or amorphous inorganic or organic materials, or a combination of these, should relax production requirements and lower the cost towards reliable, sustainable and economic electrical power from sunlight. So as to be able to compare the operation of different classes of solar cells we first summarize general photovoltaic principles and then consider implications of using less than ideal materials. In general, lower material purity means more disorder, which introduces a broad distribution of energy states of the electronic carriers that affects all the aspects of PV performance, from light absorption to the generation of voltage and current. Specifically, disorder penalizes energy output by enhanced recombination, with respect to the radiative limit, and also imposes a lowering of quasi-Fermi levels into the gap, which decreases their separation, *i.e.*, reduces the photovoltage. In solar cells based on organic absorbers, such as dye-sensitized or bulk heterojunction solar cells, vibronic effects cause relaxation of carriers in the absorber, which implies an energy price in terms of obtainable output.

1. Introduction

The use of solar cells to convert sunlight energy to electricity is increasing rapidly, but the relatively high cost of today's cells and the renewed awareness of the need to increase the use of direct solar energy have given a new boost to research in photovoltaics (PV). Alongside progress in development of more established

solar cell types, newer cell types that involve organic, molecular or polymeric materials, in some cases with nanostructured inorganic ones, are researched intensively,^{1,2} as they hold the promise of drastic cost decreases. With the steady improvement in the performance of these cells, especially those involving organic polymers, the question arises if we can define the limits for organic material-based cells, as was done for inorganic, "classical" cells. This issue is important as it can set practical goals, allow for realistic prognoses for their use and avoid over-selling. The question is not relevant just to PV, as it has been considered also for natural photosynthesis and is of direct interest for artificial photosynthesis.

The physical limits for conversion of radiation into electrical power have been given by Shockley and Queisser (SQ) half

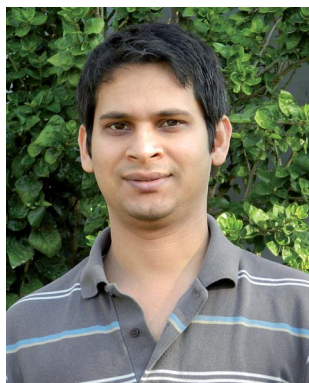
^aDept. of Materials and Interfaces, Weizmann Inst. of Science, Rehovot, 76100, Israel

^bPhotovoltaic and Optoelectronic Devices Group, Dept. de Física, Univ. Jaume I, 12071 Castelló, Spain

^cDept. of Electrical Engineering, Princeton University, Princeton, NJ, 08544, USA. E-mail: david.cahen@weizmann.ac.il; bisquert@fca.uji.es

Broader context

To what extent can *structural disorder* affect the performance of a solar cell? Answering this question is critical for estimating the limits of evolution of solar cells that are based on materials that are not ideal single crystals. After decades of research and development, solar cells, based on inorganic disordered material(s), lag behind their more crystalline counterparts in efficiency (and in commercialization), even though they allow for simpler production. While in general lower material purity means more disorder, there are also PV materials that are structurally disordered to start with or that solidify in a disordered arrangement (static disorder), all of which introduce electronic energy states in the forbidden gap near what would be band edges for crystalline materials, so-called *tail states*. Specifically, disorder decreases the electrical energy output from solar cells because of enhanced recombination, with respect to the radiative limit. In addition disorder imposes a limit on to how much the quasi-Fermi levels can be separated, *i.e.*, what is the attainable photovoltage. With solar cells based on organic absorbers, such as bulk heterojunction or, to a lesser extent, dye-sensitized cells, vibronic effects (dynamic disorder) cause relaxation of carriers in the absorber, which implies an energy price in terms of obtainable output. By analyzing these effects we show that there are basic physico-chemical limitations to the photovoltaic effect, because of both their static and dynamic disorder.



Pabitra K. Nayak

Pabitra K. Nayak is a Post-doctoral Fellow in David Cahen's group at Weizmann Institute of Science. He received his MSc degree in Chemistry from Utkal University, Bhubaneswar, India. In his PhD (from Tata Institute of Fundamental Research; TIFR, Mumbai, India) he worked on synthesis, photo-physics and electroluminescence of Organic Molecules. His current research interest is on interfacial energetics and its effect on photovoltaic performance.



Germà Garcia-Belmonte

Germà Garcia-Belmonte (1964) received his PhD degree at UNED, 1996. He worked from 1988 at CIEMAT, Madrid, on experimental and theoretical research in the area of digital processing of nuclear signals. He joined the Universitat Jaume I, Castelló, in 1992 and currently works as Professor of Applied Physics (2010) at the Department of Physics (Photovoltaic and Optoelectronic Devices Group). Recently he follows research in various topics within the field of Organic Electronics

and photovoltaics as electronic mechanisms in organic light-emitting diodes, organic photovoltaics, and plastic and thin-film solar cells. Device physics using impedance spectroscopy (including modeling and measuring) is his main subject.



Antoine Kahn

Antoine Kahn, native of France, is a Professor of Electrical Engineering at Princeton University. His group works in the general areas of semiconductor surfaces and interfaces. Over the past decade and a half, he has investigated the structural, electronic and chemical properties of surfaces and interfaces of intrinsic and doped organic molecular and polymer films, with applications to organic electronics. He has published over 330 regular and review articles.

He was the recipient of a Presidential Young Investigator Award (1984–85), and of the Weston Visiting Professorship (2009–12), Weizmann Institute of Science, Israel. He is a Fellow of the AVS (1999) and APS (2002).

a century ago.³ The SQ limit basically focuses on the properties of the absorber material, which is taken as a semiconductor with a sharp optical absorption edge (*well-defined* bandgap, E_g), so that all photons with energy larger than E_g are absorbed. Furthermore the device is considered to have unit quantum yield for conversion of absorbed photons to electrons, and infinite carrier mobilities. The question is to determine how many of the generated electrons can be extracted according to physical principles, and this is determined by the detailed balance between incoming radiation, emission by radiative recombination and the current that is generated.

Solar cells based on high-quality single crystal Si and GaAs have been constructed that approach the SQ limit to $\sim 90\%$.^{4,5} However, efficiencies of all other types of cells, and especially of those that use organic molecules, dye-sensitized solar cells (DSC), and organic photovoltaics (OPV), are far from their SQ limits as defined by the properties of their photon absorbers.

For a given solar cell the question then is, how good can we expect it to be? There are two levels of answers to this question. On the scientific level, one can determine the conversion efficiency of the cell that is irradiated by the sun on the earth's surface. Because



Juan Bisquert

Juan Bisquert is a professor of Applied Physics at Universitat Jaume I (Castelló, Spain) where he leads the Group of Photovoltaic and Optoelectronic Devices. His present research activity is focused on understanding mechanisms of devices for production and storage of clean energies, based on nanoscale semiconductors and organic materials, in particular dye-sensitized solar cells, organic solar cells, quantum dot solar cells, and solar fuel production involving water splitting with semiconductors.



David Cahen

David Cahen (BSc Chemistry and Physics, Hebrew University of Jerusalem, HUU; PhD Materials Chemistry, Northwestern Univ., PD in biophysics of photosynthesis at HUU and Weizmann Institute of Science, WIS) aims, in his research, to understand electronic transport across hybrid molecular/non-molecular, (bio)organic/inorganic materials, including proteins, with emphasis on interface energetics. In parallel, and also as part of this effort, he pursues alternative sustainable

energy resources, in particular solar cells. Novel science, which may well be somewhat iconoclastic, is of particular interest, as in his past work on 2nd generation PV. He heads the WIS' Alternative Sustainable Energy Research Initiative.

of the space and time variability of the solar radiation (insolation) we use a reference spectrum that corresponds to a total irradiation power density of 100 mW cm^{-2} (see below).

Working with small, laboratory cells allows us to test the materials and processes and to find the available efficiency for a certain combination of materials. While this is the case that we will be concerned with in this review, there are many additional issues that are important for the final goal, the practical use of the cell for electrical power generation. Except for uses with strongly concentrated sunlight, the cell has to be larger than some minimal size, so that practically it is possible to build modules. It also has to be stable during prolonged operation under sunlight. Finally, cell fabrication should have an acceptable yield (*i.e.*, the fraction of the cells/modules that are fabricated and are within the performance specifications) to make its manufacture economically viable.

Before we consider the possible extra factors that need to be taken into account to understand the gap between SQ and actual efficiencies of most cells (Sections 3–6), we will first provide a background for the photovoltaic process in Section 1, which is a short tutorial of the main steps in photovoltaic energy conversion, from light absorption to production of voltage and current, using a blackbody radiator as a model light source to determine the power conversion efficiencies. This is followed by Section 2 where we describe the main types of solar cells and Sections 3 and 4 where we analyze how disorder imposes further limits on photovoltaic conversion efficiency, which then allow us to provide a brief outlook on the future in Sections 5 and 6.

We note that in this perspective we do not touch upon various, mainly optical, approaches to try to overcome or bypass the S–Q limit. For a recent tutorial the reader is referred to ref. 6.

1.1 Blackbody radiation and solar radiation

Blackbody (BB) radiation is a thermalized radiation. The radiative emission of certain natural or artificial bright objects such as the sun or the tungsten filament of a light bulb is well described by the spectrum of BB radiation. The distribution of photons in thermalized radiation is given by the Bose–Einstein distribution function. To consider the interaction of photons with a semiconductor it is useful to express the distribution in terms of the energy of the photons, E . The photon flux, emitted by a blackbody at temperature T into a hemisphere, per unit energy interval, per unit area of emitting surface, is

$$\phi_{\text{ph}}^{\text{bb}}(E) = \frac{2\pi}{h^3 c^2} \frac{E^2}{e^{E/k_{\text{B}}T} - 1} \quad (1)$$

where h is Planck's constant, c is the speed of light, and k_{B} is Boltzmann's constant. The energy flux associated with eqn (1) can be written as

$$\phi_E^{\text{bb}}(E) = \frac{15\sigma E^3}{\pi^4 k_{\text{B}}^4} \frac{1}{e^{E/k_{\text{B}}T} - 1} \quad (2)$$

with $\sigma = 3.54 \times 10^{11} \text{ eV m}^{-2} \text{ K}^{-4}$ being the Stephan–Boltzmann constant. The total energy flux into the hemisphere is

$$\phi_{E,\text{tot}} = \frac{15\sigma}{\pi^4 k_{\text{B}}^4} \int_0^\infty \frac{E^3}{e^{E/k_{\text{B}}T} - 1} dE = \sigma T^4 \quad (3)$$

The efficiency of solar cells is calculated as the output electrical power density (see below) with respect to the received photon

energy across the whole spectrum. If blackbody radiation is arriving on a solar cell, situated perpendicular to the radiation, then the energy flux will be reduced by the solid angle that the solar cell forms, $d\Omega$, as

$$\phi_{E,\Omega} = \sigma T^4 \frac{d\Omega}{\pi} \quad (4)$$

The extraterrestrial solar spectrum is described by the standard AM0 reference spectrum, which is approximately similar to that of a blackbody at temperature 5800 K. The solar constant, f , is a standard measure of the average energy received from sunlight, and is defined as the energy received per unit time per unit area at the earth's mean distance from the sun. The integrated spectral irradiance of ASTM E-490 (standard AM0 reference) is made to conform to the accepted value of the solar constant, which is $f = \phi_E^{\text{AM0}} = 1366.1 \text{ W m}^{-2}$.

Most relevant for solar energy conversion is the terrestrial solar spectral irradiance on the surface that differs from the extraterrestrial irradiation (AM0) due to the effect of filtering by the atmosphere (Fig. 1). Air Mass 1.5 Global (AM1.5G) describes the radiation arriving at earth's surface after passing through 1.5 times a standard air mass, with the sun at 48.2° from zenith, including both direct and diffuse radiation (standard air mass is that traversed with sun directly overhead, *e.g.*, on the equator at midday in mid-summer). The AM1.5 Global spectrum (ASTM G173) has an integrated power of

$$\phi_E^{\text{AM1.5G}} = 1000 \text{ W m}^{-2} = 100 \text{ mW cm}^{-2} \quad (5)$$

This is the power density that is usually referred to as “one sun”. The AM1.5G spectrum differs markedly from the BB spectrum, especially due to two effects: the atmospheric extinction of the incoming radiation affects the shorter frequencies more than the red part of the spectrum because scattering disperses the blue light and, selective absorption by low concentration gases causes a strong decrease or total extinction

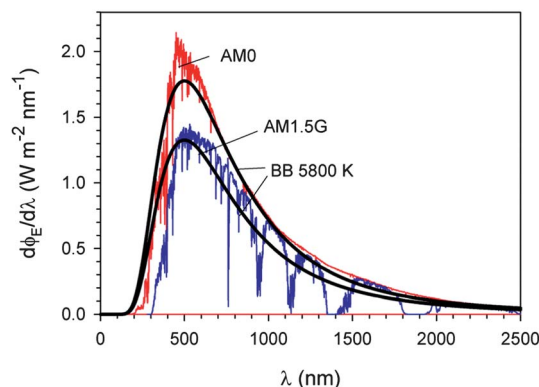


Fig. 1 The spectral irradiance (energy current density, per wavelength interval) from the sun just outside the atmosphere (AM 0 reference spectrum) and (AM1.5G) terrestrial solar spectrum. The lines are reference spectra of a blackbody at $T = 5800 \text{ K}$, normalized to a total power density of $\phi_E^{\text{AM0}} = 1366.1 \text{ W m}^{-2}$ and $\phi_E^{\text{AM1.5G}} = 1000 \text{ W m}^{-2}$.

in certain specific ranges of wavelengths, especially in the infrared region, as indicated in Fig. 1.

Nonetheless for a quantitative discussion of solar cell efficiencies it is useful to adopt the BB spectrum at $T_S = 5800$ K, as a reference. According to eqn (4) the BB spectrum must be normalized, in this case to the standard value 1000 W m^{-2} . Hence the photon flux incident on a solar cell on earth is approximated by the expression

$$\phi_{\text{ph}}(E) = F_S \phi_{\text{ph}}^{\text{bb}}(E) = F_S \frac{15\sigma}{\pi^4 k_B^4} \frac{E^2}{e^{E/k_B T_S} - 1} \quad (6)$$

where

$$F_S = 1.56 \times 10^{-5} \quad (7)$$

Of course more detailed and accurate calculations of solar cell efficiency are obtained using the AM1.5G spectrum for $\phi_{\text{ph}}(E)$. In practical determination of the efficiencies, the lamp simulating AM1.5G should be carefully calibrated, and this is often a cause of concern.⁷

1.2 The absorber

Direct generation of electrical energy from sunlight requires transferring as much as possible of the photon energy to electronic energy by exciting electrons in the light-absorbing material. This material can be organic or inorganic, semiconductor or non-molecular (periodic lattice, polymer, amorphous) or a molecular dye. In terms of its optical properties we are particularly interested in its absorbance $a(E)$ (absorbance = $\alpha(E)l$, where α is the extinction coefficient and l is the thickness). Semiconductors are characterized by an absorption edge, their bandgap, E_g ; photons with energies $< E_g$ are not absorbed and photons with energies $> E_g$ are absorbed, *with increasing absorbance as their energy increases*. This last property does not hold for molecules and molecular materials. For example Chlorophyll *a* absorbs strongly around 430 and 660 nm but relatively weakly in the range between these wavelengths (as well as at energies > 630 nm). Still, if a thick enough film of either type of material is used all photons with energies above the absorption edge will indeed be absorbed.

For simplicity we will consider for the moment, as in the SQ approach, a semiconductor that absorbs all photons of energy $> E_g$ ($a(E) = 1$ for $E \geq E_g$). Fig. 2(a) shows as an example the photons absorbed for a semiconductor of bandgap $E_g = 1.5$ eV. Once the photon is absorbed (process 1 in Fig. 3(a)), there is a rapid relaxation of the exciton, or separated electron and hole carriers, to the lowest energy configuration, E_g , in this example (process 2 in Fig. 3(a)). Meanwhile, the photons with energy $< E_g$ are not absorbed. Therefore, after the fast thermalization of photogenerated carriers in the absorber, the energy available is E_g for each absorbed photon. The loss of unabsorbed photons and loss of the energy $E - E_g$ of the absorbed ones are the main causes for the low efficiency of the quantum conversion of sunlight energy into electrical energy (as contrasted to conversion to thermal energy only). Fig. 2(b) shows that $>50\%$ of the BB radiation energy at T_S is lost even under the most favorable condition, which is $E_g \cong 1.1$ eV.

1.3 Generation of electrical power

To be able to generate electrical power, P_{el} , the absorber is made part of an arrangement with additional materials so that electron-hole pair creation results ultimately in the generation of electrical current, I_{el} , and voltage, V , with

$$P_{\text{el}} = I_{\text{el}}V \quad (8)$$

By measuring, under illumination, the current as a function of voltage we get the I - V characteristic of the cell. By normalizing for the illuminated area, we find the current density, with which we get the j - V characteristic (Fig. 4(a)). These characteristics show the two central aspects of the photovoltaic generation of electrical power. The first is the photocurrent, basically the extraction of the photogenerated electrons and holes. The second is the voltage at which the electrons and holes are extracted, which is the difference of the electrochemical potentials (quasi-Fermi levels) of the electrons and holes in the materials. There is a tradeoff between current and voltage. At low voltage, current extraction is easy, and the current is determined by the quantum yield (conversion of photons to electron carriers) of the absorber. At high voltage the recombination current, which flows against the photocurrent, increases until the power starts to decrease, reaching zero at the open circuit voltage, where the light-induced

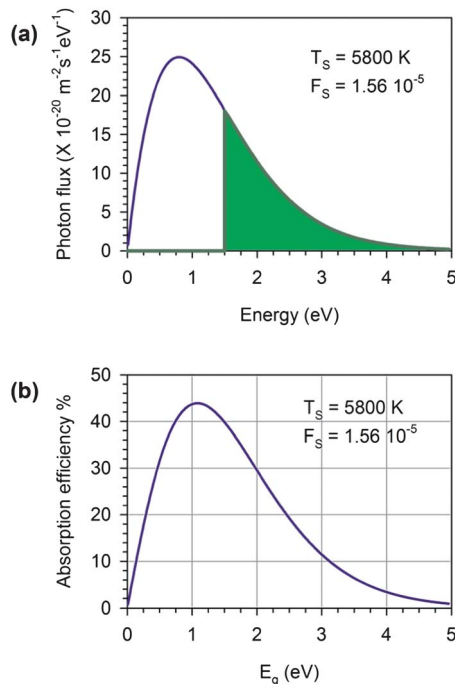


Fig. 2 (a) Photon flux emitted by a blackbody at 5800 K, normalized to a total emitted power of 1000 W m^{-2} , the standard value for the terrestrial solar spectrum. The shaded area indicates the photons absorbed by a semiconductor of bandgap $E_g = 1.5$ eV and absorbance $a = 1$. (b) Estimation of the power conversion efficiency that considers only two factors—loss of sub-bandgap photons and relaxations—of electron-hole pairs to the bandgap energy. The calculations count at each energy the absorbed photon flux, *i.e.*, photons with energy $\geq E_g$, each photon contributing energy E_g . This energy is divided by the total power flux of the blackbody radiation. This estimate neglects several important characteristics of actual physical converters, as is discussed in the main text. F_S is the factor that normalizes the emitted flux to 1 kW m^{-2} .

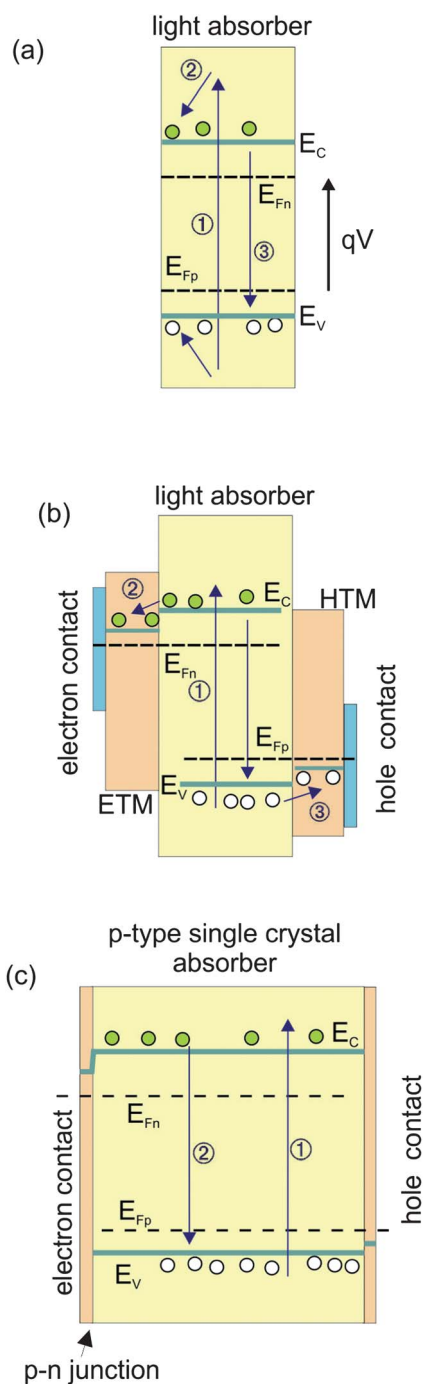


Fig. 3 (a) Absorption of light in a semiconductor (1) produces electrons and holes that rapidly relax (2) to the bottom of the conduction band (E_C) and top of the valence band (E_V). The excess photogenerated carriers produce a splitting of the quasi-Fermi levels of electrons (E_{Fn}) and holes (E_{Fp}). Electrons relax to the valence band by recombination with holes (3). (b) The addition of electron and hole selective contacts by electron and hole transport materials allows the extraction of voltage and current. (c) In a thick monocrystalline p-type Si absorber the electron selective contact is formed by a p-n junction.

and dark currents cancel. In between the extreme cases of low and high voltage lies V_{mp} , the voltage at which the generated electrical power is maximum and which yields the cells' stated efficiency (its best possible one; cf. Fig. 4(b)):

$$\eta = \frac{j_{mp} V_{mp}}{\phi_{E, tot}} \quad (9)$$

1.4 Generation of photocurrent

To evaluate the maximum electrical current that can be produced by a material with a sharp absorption edge at the energy E_g , we assume that each absorbed photon is converted to one electron. We integrate for all the photons of energy larger than the bandgap of the absorber (cf. eqn (3))

$$J_{ph, tot} = F_S \frac{15\sigma}{\pi^4 k_B^4} \int_{E_g}^{\infty} \frac{E^2}{e^{E/k_B T_S} - 1} dE \quad (10)$$

With a change of variables $x = E/k_B T$, the electrical current from all the absorbed photons is

$$j_{el} = q J_{ph, tot} = q F_S \frac{15\sigma T_S^3}{\pi^4 k_B} \int_{x_g(T_S)}^{\infty} \frac{x^2}{e^x - 1} dx \quad (11)$$

where q is the elementary charge and

$$x_g(T_S) = \frac{E_g}{k_B T_S} \quad (12)$$

The maximum current density that can be obtained from this type of BB radiation is $j_{el} = 73 \text{ mA cm}^{-2}$. The current as a function of the absorption edge, the semiconductor bandgap here, is shown in Fig. 5(a). The currents for AM1.5G insolation are also shown in Fig. 5(a). The maximal current, obtainable with an $E_g = 1.1 \text{ eV}$ absorber, is $\sim 43 \text{ mA cm}^{-2}$.

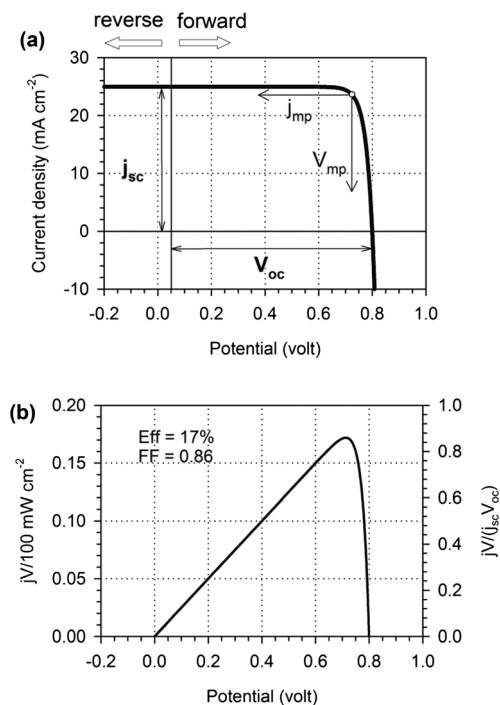


Fig. 4 Theoretical calculation of the current-potential curve (a) and power output (b) of a solar cell with $j_{sc} = 25 \text{ mA cm}^{-2}$, $V_{oc} = 0.8 \text{ V}$, and using a Shockley diode model with a diode factor $n = 1$. In (b) the left vertical axis gives the output power density, normalized to the incident power density of 1 sun (AM1.5G) and, thus, gives the conversion efficiency; the right axis gives the fill factor.

1.5 Generation of photovoltage

According to thermodynamics, the energy that can be converted to useful work is the free energy, and the free energy per carrier is the chemical potential, (the electrochemical potential, in the presence of an electric potential difference) or Fermi level. As shown in Fig. 3(b), the creation of excess electrons and holes produces a separation of the quasi-Fermi levels, E_{Fn} and E_{Fp} , for electrons and holes, respectively, in the absorber. This mechanism is rather general and is illustrated for the case of a standard Si solar cell in Fig. 3(c) that is discussed later on. The photovoltage is given by

$$qV = E_{Fn} - E_{Fp} \quad (13)$$

It is obvious that we cannot extract voltage (or current) just from a piece of light-absorbing material. We need contacts so that carriers can be removed from the system to flow out and through an external circuit to do the work that we desire. Here the meaning of “contact” is extended to include a combination of materials that perform the required function of conversion of the excess generated carriers in the absorber into electrical power in an outer circuit. The contacts to the absorber are key elements in a solar cell.^{8,9}

If these contacts behave ideally, then the current–potential characteristic is well described by the Shockley diode model:

$$j = j_{sc} - j_0[e^{qV/nk_B T} - 1] \quad (14)$$

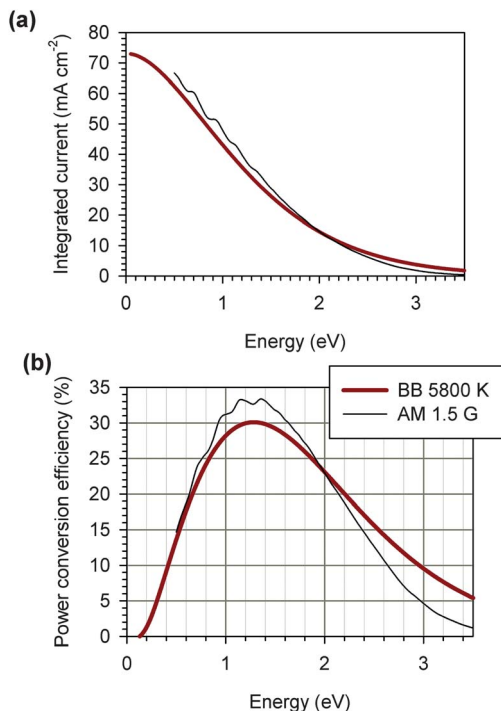


Fig. 5 (a) Integrated current as a function of the bandgap energy of the absorber, for incident blackbody radiation at temperature $T_S = 5800$ K, with total energy flux $\phi_{E,\text{tot}} = 1000$ W m⁻². (b) The maximal photovoltaic efficiency of the absorber, assuming FF = 0.83. The thin lines are the current and Shockley–Queisser efficiencies for actual AM1.5G solar irradiance.

Here j_{sc} is the short-circuit current, j_0 is the reverse current, corresponding to thermal generation of carriers, and n is the diode ideality factor. In the SQ limit, j_{sc} can be equated with j_{el} , and the thermal generation current, which determines j_0 , can be obtained from light emission properties of the absorber. In the SQ model all recombination is associated to radiative emission and the detailed balance assumption relates the luminescence to the blackbody spectrum at the ambient temperature of the solar cell, T_a . The open-circuit voltage is given by

$$V_{oc} = \frac{nk_B T}{q} \ln \left(\frac{j_{sc}}{j_0} + 1 \right) \quad (15)$$

One limit to the open-circuit voltage, V_{oc} , is the bandgap energy E_g . This is because the transport bands have extended states with a high density and except for extreme conditions that are not relevant for solar cells, the quasi-Fermi levels cannot move into the conduction and valence band edges. However, the actual V_{oc} is determined by recombination at open circuit, and will be $< E_g$ at one sun, as obtained from detailed balance of generation and emission in SQ limit. This is expressed in eqn (15). In practical solar cells additional recombination pathways further decrease V_{oc} below the SQ limit value. In addition, as already mentioned the solar cell must be operated at some voltage below V_{oc} . This implies a reduction of power with respect to the product $j_{el}V_{oc}$, a reduction, given by the fill factor (FF). The FF can be described empirically by the expression:¹⁰

$$FF = \frac{v_m}{v_m + 1} \frac{v_{oc} - \ln(v_m + 1)}{v_{oc}(1 - e^{-v_{oc}})} \quad (16)$$

where $v_{oc} = V_{oc}/nk_B T$ and $v_m = v_{oc} - \ln(v_{oc} + 1 - \ln v_{oc})$.

FF decreases with increasing values of the diode quality factor, which is essentially related to the recombination mechanism in the solar cell (once series resistances are removed).¹¹

The electrical power provided by the solar cell at the maximum power point is

$$\eta = \frac{j_{el} FF(V_{oc}) V_{oc}}{\phi_{E,\text{tot}}} \quad (17)$$

Calculations of the efficiency in SQ limit are shown in Fig. 5(b), both for BB radiation at $T = 5800$ K and for AM1.5G solar spectrum.

To summarize, in the SQ model the current obtained is j_{el} , eqn (11), and there are two main causes that make the efficiency less than $j_{el}E_g/\phi_{E,\text{tot}}$ (plotted in Fig. 5(b)). The first is recombination at open circuit, that makes $V_{oc} < E_g$, and the second is a further reduction of current and voltage at the maximum power point, given by the FF.

In Section 2 we will discuss how each of the parameters V_{oc} , J_{sc} and FF behaves when we use disordered materials for solar cells and how they compare to their crystalline counterparts.

1.6 Determining radiative limit to photovoltage from external quantum efficiency

Although the SQ efficiency limit is taken as a universal measure to gauge efficiencies of different solar cell technologies, the fact is that for many cell types it presents only the first step.¹² Thus, the assumption of abrupt absorption at a certain E_g value does not match well the properties of absorber materials that are not high

quality single crystals (*i.e.*, all 2nd and 3rd generation solar cells and the a-Si:H cells), especially if these are molecular and polymeric organic materials of the type used in DSC and BHJ solar cells.

A useful method to determine the absorption and charge collection properties of the solar cell that are relevant for energy conversion is to measure the short-circuit current under monochromatic light as a function of wavelength, divided by the theoretical current associated with the incident photon flux:

$$\eta_{\text{EQE}}(\lambda) = \frac{j_{\text{sc}}(\lambda)}{q\phi_{\text{ph}}(\lambda)\Delta\lambda} \quad (18)$$

This magnitude is termed the external quantum efficiency (EQE) or incident-photon to current conversion efficiency (IPCE). Having determined the EQE, the short-circuit photocurrent under one sun illumination should correspond to

$$j_{\text{sc}} = q \int_{\lambda_{\text{min}}}^{\lambda_{\text{max}}} \eta_{\text{EQE}} \phi_{\text{ph}}^{\text{AM1.5}}(\lambda) d\lambda \quad (19)$$

where λ_{min} and λ_{max} are the wavelengths where the EQE vanishes. An example of measured EQE of a DSC with 11.7% power conversion efficiency at 1 sun is shown in Fig. 6(a),¹³ in combination with the photon flux of the AM1.5G spectrum. The integration of eqn (19) gives, based on the experimentally

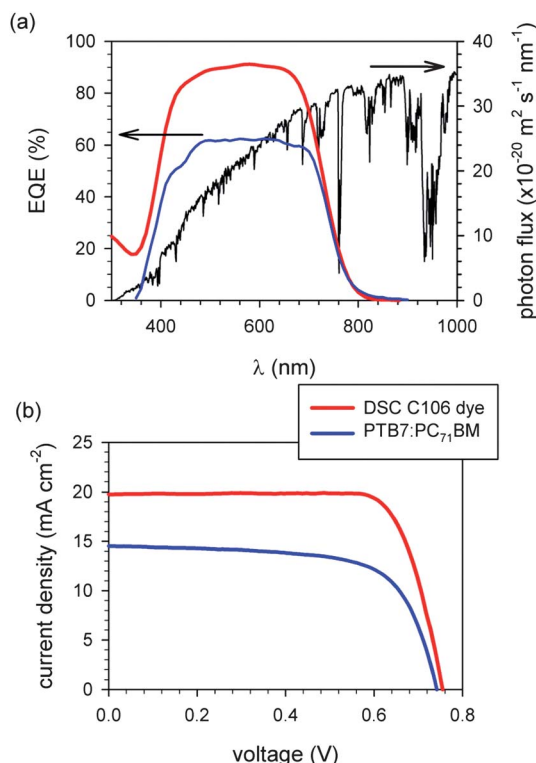


Fig. 6 (a) Air Mass 1.5 Global (AM1.5G) solar spectrum (photon flux as a function of wavelength) and the measured External Quantum Efficiency (EQE) of a DSC with C106 dye (data courtesy of M. Zhang and P. Wang, Changchun Institute of Applied Chemistry) and of a BHJ solar cell formed by PTB7:PC₇₁BM (data courtesy of I. Murray, S. Loser, M. Hersam, T. J. Marks and L. Yu, Northwestern University and University of Chicago). (b) Current density–potential characteristics of the cells at simulated AM1.5G illumination.

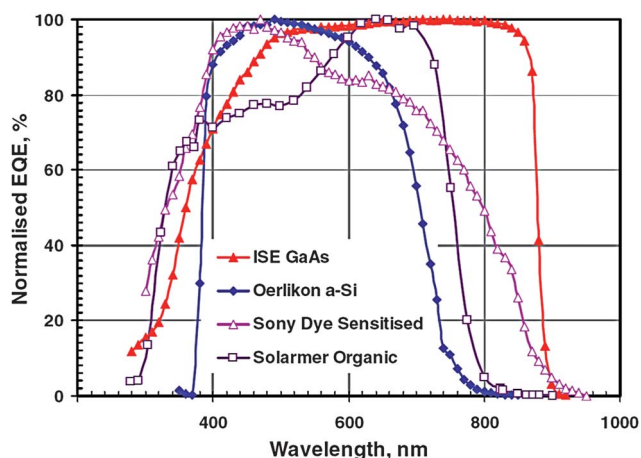


Fig. 7 External Quantum Efficiency (EQE) spectra for different types of “best” photovoltaic cells (reproduced with permission from ref. 69, © 2010, John Wiley and Sons).

measured EQE for this case, 18.95 mA cm⁻², in good agreement with the measured photocurrent, as shown in Fig. 6(b). As an example of the BHJ solar cell, we show the EQE of a PTB7:PC₇₁BM solar cell with 7.5% PCE.¹⁴ Examples of the EQE of several other cells are given in Fig. 7. It is clear that EQE of the a-Si:H, DSC and BHJ cells does not fit well with the SQ assumption of an abrupt bandgap (as exemplified by the GaAs cell in Fig. 7).

It would be interesting therefore to determine a theoretical efficiency starting from the real EQE. Ross¹⁵ established the maximal voltage that a solar cell of arbitrary absorbance can provide under illumination, based on the balance of the incoming radiation from ambient blackbody radiation, $\phi_{\text{ph}}^{\text{bb}}(\lambda, T = 300 \text{ K})$, and the luminescent emission of the absorber. Recently Rau and Kirchartz^{16,17} related the electroluminescent emission $\Delta\phi_{\text{em}}$ at a certain voltage, V , to the exponentially enhanced blackbody radiation, for a material that has an arbitrary EQE, as follows:

$$\Delta\phi_{\text{em}} = \eta_{\text{EQE}}(\lambda) \phi_{\text{ph}}^{\text{bb}}(\lambda) \left[\exp\left(\frac{qV}{k_{\text{B}}T}\right) - 1 \right] \quad (20)$$

The minimal recombination current of a solar cell is¹⁷

$$j_{0,\text{rad}} = q \int_0^{\infty} \eta_{\text{EQE}} \phi_{\text{ph}}^{\text{bb}}(\lambda) d\lambda \quad (21)$$

Using eqn (15), the radiative limit to the photovoltage is

$$V_{\text{oc}}^{\text{rad}} = \frac{k_{\text{B}}T}{q} \ln \left(\frac{j_{\text{sc}}}{j_{0,\text{rad}}} - 1 \right) \approx \frac{k_{\text{B}}T}{q} \ln \left(\int_0^{\infty} \eta_{\text{EQE}} \phi_{\text{ph}}^{\text{AM1.5}}(\lambda) d\lambda / \int_0^{\infty} \eta_{\text{EQE}} \phi_{\text{ph}}^{\text{bb}}(\lambda) d\lambda \right) \quad (22)$$

But the actual photovoltage is less due to the additional non-radiative pathways for recombination, the loss due to which is expressed as^{15–17}

$$V_{\text{oc}}^{\text{rad}} - V_{\text{oc}} = -\frac{k_{\text{B}}T}{q} \ln \left(\frac{j_{\text{rad}}(V_{\text{oc}})}{j_{\text{rad}}(V_{\text{oc}}) + j_{\text{nonrad}}(V_{\text{oc}})} \right) \quad (23)$$

This approach has been applied to discuss the efficiency of III–V¹⁸ and organic solar cells.¹⁹

If the collection efficiency of the solar cell is reasonably large, the photocurrent is balanced by the recombination current at open circuit. The external radiative efficiency (ERE) at open circuit is

$$\text{ERE} = \frac{\exp\left(\frac{qV_{\text{oc}}}{k_{\text{B}}T}\right) \int_0^{\infty} \eta_{\text{EQE}} \phi_{\text{ph}}^{\text{bb}}(\lambda) d\lambda}{\int_0^{\infty} \eta_{\text{EQE}} \phi_{\text{ph}}^{\text{AM1.5}}(\lambda) d\lambda} \quad (24)$$

A recent calculation by Green²⁰ of a broad collection of solar cell classes shows that solar cells based on organic materials have the lowest EREs. As discussed later on, this behavior is primarily due to the existence of several parallel recombination pathways in addition to recombination through the absorber, which, by itself, represents only 10^{-6} of the total recombination.

2. Realizations of solar cells with a single absorber material¹²

The previous analysis emphasized the fact that the limits to photoelectric conversion, set by the SQ limit or its extensions, are entirely determined by the properties of the absorber, *i.e.*, the light absorption and radiative emission. The current–potential curve is simply a statement of recombination as a function of voltage for an absorber *with perfect selective contacts*.

How well do real solar cells approach this maximal performance? To answer this question the main point is the arrangement of materials to provide a mechanism of charge separation. Basically, if charge separation occurs in the absorber itself, the SQ limit can be approached.

2.1 “First generation” solar cells

The so-called “first generation” solar cells are based on crystalline inorganic materials like Si (1.12 eV), GaAs (1.42 eV) and InP (1.28 eV). A scheme of a p–n type crystalline silicon solar cell is shown in Fig. 3(c). In the crystalline silicon solar cells the thickness of the absorber is $\sim 200 \mu\text{m}$. This material is of course supplemented with selective contacts, which are a p–n junction as electron extraction contact and a highly p-doped (P^+) layer as hole extraction contact. But the thickness of these layers is several hundred nm, at most, and their sizes are entirely negligible with respect to the absorber. As a result, the thermalized carriers that determine the positions of Fermi levels occur mostly in the absorber itself, and provided that defects are well passivated at the surface, recombination also occurs in the bulk absorber material. Therefore, the crystalline silicon solar cell should be able to approach in practice the SQ limit. The record Si solar cell yields 43.3 mA cm^{-2} photocurrent under AM1.5G insolation.^{5,12} Because the Si bandgap is 1.12 eV, this is practically at the limit of photon to electron conversion efficiency (see Fig. 5(a)). The V_{oc} of this cell is 0.71 V. There are similar high values for single crystalline GaAs cells with a photocurrent of 29.4 mA cm^{-2} and a V_{oc} of 1.11 V.⁵ InP based solar cells have slightly lower photocurrent efficiency (29.5 mA cm^{-2}) with a V_{oc} of 0.88 V,⁵ which can be ascribed to the smaller development efforts invested in them. In these types of cells the practical limits of PV efficiency appear to have been achieved or at least closely approached. Yablonovitch *et al.* have recently emphasized that

the limitations to reach the maximal SQ performance in crystalline solar cells are due to losses in open-circuit voltage.¹⁸

However, as these cells require high-quality crystalline materials (and, for Si, a relatively large amount of material, so as to assure total optical absorption, because Si is an indirect bandgap material, *i.e.*, has a low absorption coefficient over much of the range where it absorbs) they are still expensive, in terms of the price of electrical energy that they generate, compared to conventional methods of electrical power generation. Additionally, the energy payback time for these types of cells is still measured in years, rather than months (or weeks as for some coal-fired power plants).

2.2 Cells, based on inorganic materials with structural disorder

The cost of solar cell production can be reduced if we use polycrystalline or amorphous absorbers, because of decreased cost of materials. We will first consider inorganic material-based cells of this type.

Mostly, these cells are based on Si, in forms from amorphous (a-Si), to nano-, micro-, poly- and multi-crystalline (nc-Si, $\mu\text{c-Si}$, pc-Si, mc-Si; typical grain sizes are nm, μm , 10–100 μm and mm to cm), on copper indium gallium diselenide (Cu(In,Ga)Se_2 , CIGS) or on cadmium telluride (CdTe). Disorder in these materials affects both the photocurrent and photovoltage efficiencies.

Photocurrent efficiencies in these cells are between 80 and 85% of the maximum achievable current for the E_{g} of the material used, significantly lower than for single crystal-based cells.¹² The main reason for this decrease is the lower mobility of the minority carriers, due to scattering at grain boundaries (GBs). The causes are both the abrupt structural change at the GBs and the fact that impurities often segregate there. In recent years, nm scale studies have shown how these losses can be accounted for by the GBs’ chemistry and physics.

Fig. 8 is a schematic band/energy level diagram of a solar cell with a polycrystalline material as absorber. The principle of operation is similar to that of a single crystal-based cell (Fig. 3(c)), but the presence of grain boundaries (green stripe with slight downwards bent bands), or defects in general, introduces energetically preferred recombination pathways. As a result the cell’s performance departs more and more from the band-to-band radiative recombination model.

In most cases the GB results in a barrier, which translates as a resistance, and as such decreases the voltage that can be generated by the cell, because this barrier has to be overcome. There is another effect, though, that has received less attention, which is that of near band edges, tail states. The broken periodicity at the GBs introduces states in the gap, with, for a completely amorphous semiconductor, such as a-Si, a continuum of states, decreasing in density from the band edges to the centre of the gap. Such states are also present in polycrystalline materials, and their density will increase with the increase in disorder in the material/decrease in crystallinity.

Their effect is to decrease the amount of absorbed photon energy that is actually available for conversion and to decrease the achievable voltage by limiting the separation between quasi-Fermi levels that is attainable.

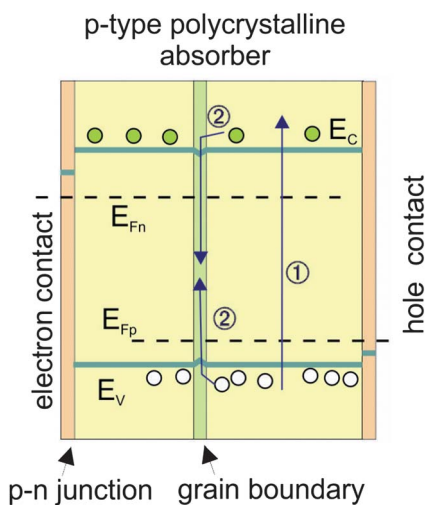


Fig. 8 Schematic energy level/band diagram of a solar cell formed by a polycrystalline material, the absorber, which is also the electron and hole transport material (*cf.* Fig. 3c for diagram of a material without grain boundary). A grain boundary, shown (in light green), with slight (downward) bending of the bands, is assumed to be the dominant carrier recombination site. The arrows indicate the following processes: (1) absorption of light, producing electrons and holes that relax to the bottom of the conduction band (E_C) and top of the valence band (E_V). The excess photogenerated carriers produce a splitting of the quasi-Fermi levels of electrons (E_{Fn}) and holes (E_{Fp}). (2) Recombination of electrons by relaxation to the valence band.

The first effect, of sub-bandgap absorption, which removes photons that could be used in a multi-cell arrangement, is negligible. Photons, absorbed into (near VB) tail states with energies that can excite an electron beyond the mobility edge, can contribute to the photocurrent. The drift mobility (and the final state) of the electron is the same, irrespective of the excitation energy²¹ and the hole present in a tail state can be mobile *via* hopping. The low cross-sections for excitation from the VB (into the CB) to near-CB (from the near-VB) tail states ($>100\times$ less than band–band transition) make these processes relatively minor ones.

The second effect concerns thermalization into the tail states of the e^-h^+ pairs, generated by $\geq E_g$ photons. As the voltage that can be extracted is determined by the quasi-Fermi level separation, this will now be decreased as tail state, rather than band (mobility) edge energies will become the relevant ones. In 1981 Tiedje analyzed the physics of a-Si:H cells and concluded that the amorphous structure of the absorber and the resulting tail states exact an extra price of several 100 mV, compared to what is the case for perfect crystalline cells.²²

We can also appreciate that in the perfect crystal, charge separation relies on the high mobility and the closely related long diffusion length that allows carriers to traverse the absorber thickness, limited only by what is primarily radiative recombination. But, as noted, the high materials cost of high quality crystalline materials leads to work on less ideal materials at the expense of the conversion efficiency. While it is likely that the efficiency of today's inorganic polycrystalline cells can be improved further, they cannot approach the SQ limit as close as the single-crystal-based cells for the reasons outlined above.

3. Cells, based on strongly disordered, organic absorber materials

3.1 Dye-sensitized solar cells (DSCs) and bulk heterojunction (BHJ) solar cells

A different route to prepare solar cells, one that has been the subject of intense research in recent years, is to use a combination of materials for the separate steps involved in the photovoltaic effect. The absorber is mixed with other materials that rapidly extract the electron and hole carriers and transport these to the electrodes. By achieving this mixing at a nanometre scale, it becomes possible to use a thick enough layer of an absorber (from 100 nm to 10 μm , depending on the extinction coefficient of the absorber) that, as single phase for sufficient optical absorption, would have too high an electrical resistance to be fruitful as PV material. The main examples of this approach of combining the absorber and the electron and hole transport materials (ETM and HTM, respectively, *cf.* Fig. 3) are the DSC^{1,23} and organic BHJ cells.^{2,24} In a BHJ, either the ETM or the HTM (in some cases both) plays the role of an absorbing layer. The ETM and HTM in a BHJ are also known as acceptor and donor, respectively.

3.2 Photon absorber

In these cells light is absorbed by a conjugated material (small organic molecule, organic polymer or organometallic molecule), rich in π -electrons. The absorption coefficients of these molecules are very high due to strong overlap of their ground and excited state wave functions. Generally, absorption leads to formation of a singlet (spin 0) excited state. These excited states quickly thermalize to the lowest vibronic state of the lowest singlet state (S_1)²⁵ in a process that is similar to thermalization of an electron that is excited into the CB and thermalizes to the CB minimum.²⁶ The energy difference between the lowest vibronic state of the ground state (S_0) and of S_1 defines the absorption edge (*i.e.* bandgap) of the molecule. The absorption spectrum of molecules is generally broad (unlike the step function of a direct transition semiconductor), due to varying degrees of coupling between the ground and different excited states. Molecules with a spectral spread in the visible and near IR parts of the solar spectrum are candidates for solar energy harvesting. In a solid film of the type, needed for complete absorption of the solar flux, the local environments of the molecules vary, which leads to further modulation of the absorption spectrum. Therefore, *it is hard to define a clear absorption edge for molecular systems*. This uncertainty directly impacts on our ability to use the Shockley–Queisser formalism to determine conversion efficiency limits and it makes the earlier-discussed Ross–Rau formalism (Section 1.6) an attractive alternative.

Due to the weak intermolecular interactions, and the low dielectric constant of organic materials, splitting the (Frenkel) exciton into a free electron and hole will be extremely inefficient if only the room temperature thermal energy, $k_B T = 26$ meV, is available. This is very different from the situation in the p/n junction cell based on inorganic materials where the (Wannier) exciton binding energy is less than $k_B T$. The Frenkel exciton binding energy is several 100 meV.²⁷ We note that there is a continuing debate about a more exact value, which, naturally, will also vary between different organic materials and in addition

can be influenced by screening by background free carriers.²⁸ This high exciton binding energy value is consistent with the experimental findings that the pure materials never have a high yield of photo-generated carriers. The central importance of this problem of exciton splitting explains why these cells are also known as excitonic solar cells.

One way to overcome the problem is to split the exciton at an interface, which can provide the necessary driving force because of differences in electron and hole energies in the two phases that form the interface. The requirement of an interface, though, puts a serious limitation on absorber thickness. The exciton should diffuse to the interface, *before* decaying to the ground state. The lifetime of excitons in the relevant materials is ~ 1 ns, which corresponds to an exciton diffusion length of ~ 10 nm. So as not to lose solar photons, because of insufficient absorption, the absorber thickness has to be at least ~ 100 nm. To overcome this dilemma of the need for too thick an absorber, the absorber can be adsorbed *as a monolayer* on a porous, very high surface area material (as in the DSC) or a bulk hetero-junction can be formed, as in organic BHJ cells. We note however that organic solar cells prepared by serial layers (based on small molecules) have also achieved significant efficiencies.^{5,9,29}

3.3 Working principles of DSC⁸

A scheme of the DSC is presented in Fig. 9. The excitation of a dye molecule by a photon promotes an electron to the excited state of the sensitizer; the electron is then rapidly injected into the TiO₂ nanostructure. The oxidized dye is regenerated by a redox carrier, a liquid electrolyte with high ionic concentration, or *via* a solid hole conductor. Efficient electron-hole separation requires an energy price, which is reflected in the electronic energy level alignment of the materials, which has to be such that it facilitates both electron injection into the conduction band of the ETM and regeneration of the oxidized dye by hole transfer to the HTM. This is in contrast to a single material (inorganic) solar cell, discussed above. The main difference is that the quasi-Fermi levels of electrons and holes, that establish the voltage in the solar cell, are not determined in the absorber (where the photoexcited carriers may not even relax before injection³⁰) but in the ETM and the electrolyte, respectively (see Fig. 9(a)). In a DSC, in contrast to what we showed in Fig. 3(c), we find that stable populations of carriers, determining the quasi-Fermi levels, occur in separate materials and not in the absorber only. Because the stable populations of photogenerated carriers occur in the ETM and HTM, charge transfer between these two media dominates recombination of carriers, as indicated in Fig. 9(a). This picture differs, therefore, in many respects from that of a single material cell, concerning the physical limits to efficiency. First of all the ETM and HTM have their own transport levels, which cannot be crossed by the quasi-Fermi level. But due to the energy steps, required for efficient carrier injection and for regeneration of the sensitizer (in a DSC), the difference between such levels is substantially less than the optical absorption gap of the absorber. There is, therefore, an *a priori* reduction of voltage by the energy required to drive injection and regeneration.

In reality, V_{oc} is determined by the number of electrons stored in the ETM, most commonly TiO₂ (titania), and this is in turn set by recombination of the thermalized electrons in the electron

transport nanostructure. Disorder in the titania nanostructure, which is prepared and made up of individual nm sized particles, with some interparticle sintering, is a prominent feature that is expressed also in the material's energy levels. These can be traced experimentally, *e.g.*, by chemical capacitance.³¹ In Fig. 9(b) we indicate the titania gap states. Experimental chemical capacitance data that reflect this energy disorder and which are characteristic for the nanoporous titania, used as ETM, in a broad collection of DSCs, using different dyes and electrolytes, are given in Fig. 9(c).³² The C_{μ} vs. V_F plots (Fig. 9(c)), where V_F reflects the electron Fermi level in TiO₂ with respect to redox potential (Fermi level equivalent) in the redox solution,³³ relate directly to the density of states, $g(E)$, at the Fermi level according to the expression

$$C_{\mu} = q^2 \frac{\partial n_L}{\partial E_{Fn}} = qg(E_{Fn}) \quad (25)$$

where n_L is the total density of electrons in localized states in the bandgap.³¹ The results in Fig. 9(c) show that the electron distribution in the bandgap obeys an exponential distribution of traps, which is shifted on the horizontal, V_F , scale, depending on the composition of the electrolyte of the particular DSC. This shift on the V_F scale reflects a shift of the conduction band position with respect to the reference, the Fermi level of the HTM, in general.

Electrons accumulated in the TiO₂ nanostructure transfer mainly to holes in the redox carrier, as suggested in Fig. 9(a), very likely by a mechanism involving transfer through surface states,^{31,34} as indicated in Fig. 9(b). These findings support the idea that disorder determines both carrier accumulation in TiO₂ and the dominant pathway for recombination. Because recombination is disconnected from radiative emission in the absorber, the external radiative efficiency is extremely low, as noted by Green.²⁰ A substantial decrease of the voltage can be expected, with respect to the radiative limit for voltage, described in Section 1.6. A scheme indicating this situation, and the different reductions of voltage in a DSC, is shown in Fig. 10.

3.4 Working principles of a BHJ solar cell

The active layer of a BHJ solar cell is a (phase segregated) blend of a hole carrier material *i.e.* the donor (D) and an electron carrier material, the acceptor (A). We will use the energy scheme of a standard BHJ solar cell, shown in Fig. 11, to discuss the mechanism of operation and the losses incurred during PV operation. Excitons are photogenerated in the organic absorber, often a thiophene-based polymer, such as P3HT (Poly-3-Hexyl-Thiophene), which is also the donor and dissociated at its interface with an electron-accepting ETM, mostly a C₆₀ derivative, by injecting an electron into it.³⁵ Some photogeneration of excitons in the fullerene can occur³⁶ and is also indicated in Fig. 11.

Charge separation using only organic materials requires more energy than that using an inorganic and organic interface as in the DSC (because now all phases have a low dielectric constant and low mobility). The rate of Photo-Induced Electron Transfer, PIET, in these materials is described by the Marcus electron transfer model.³⁷ In this model the activation energy (ΔG^*) for energy transfer is given by

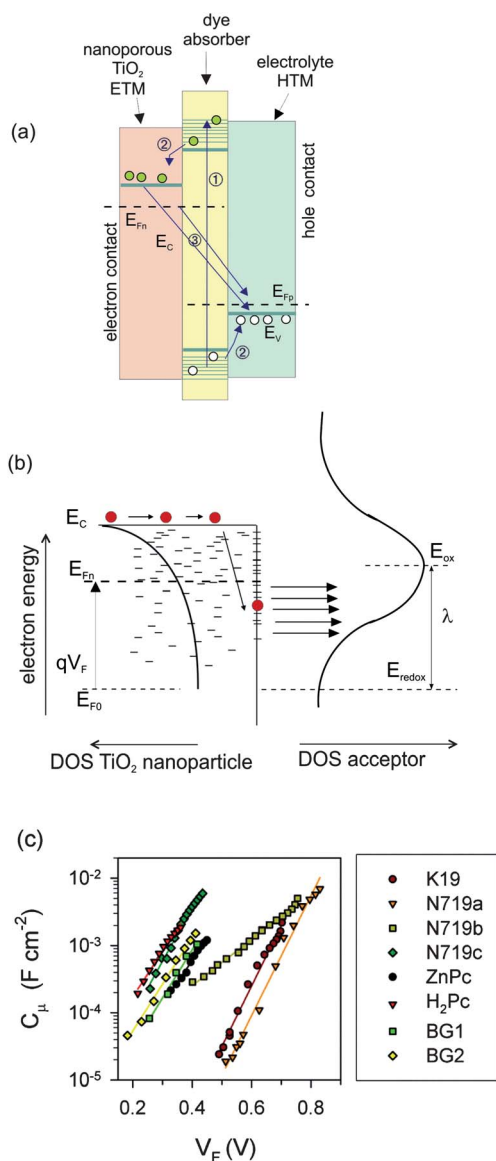


Fig. 9 (a) Energy diagram of a nanostructured solar cell (specifically a DSC), formed by several (spatially mixed) materials that function, separately or jointly, as the absorber, the electron (ETM) and hole (HTM) transport materials. The arrows indicate the following processes: (1) absorption of light, generating electrons and holes in the absorber. (2) Injection from the absorber to the ETM and HTM. Carriers relax to the conduction band of the ETM, E_C , and the valence band (E_V) of the HTM, producing a splitting of the quasi-Fermi levels of electrons (E_{Fn}) in the ETM and holes (E_{Fp}) in the HTM. (3) Recombination of electrons in the ETM with holes in the HTM, both from E_C and from bandgap surface states in the ETM. (b) Schematic representation of the steps involved in the recombination between the electrons in TiO_2 nanoparticles and the oxidized species in the electrolyte (or hole conductor). E_{F0} is the position of the Fermi level in the dark, equilibrated with the redox potential E_{redox} (the redox solution equivalent of the Fermi Level³³) of the acceptor species in solution. The following processes are indicated: electron transport in the transport level; capture by surface states; and electron transfer through a surface state. On the right side we show the fluctuating energy levels of oxidized species in solution according to the Marcus–Gerischer model.^{37,70} λ is the reorganization energy of the acceptor species in the ionic or hole transport material with an effective density of states D . E_{ox} is the most probable energy level for the oxidized

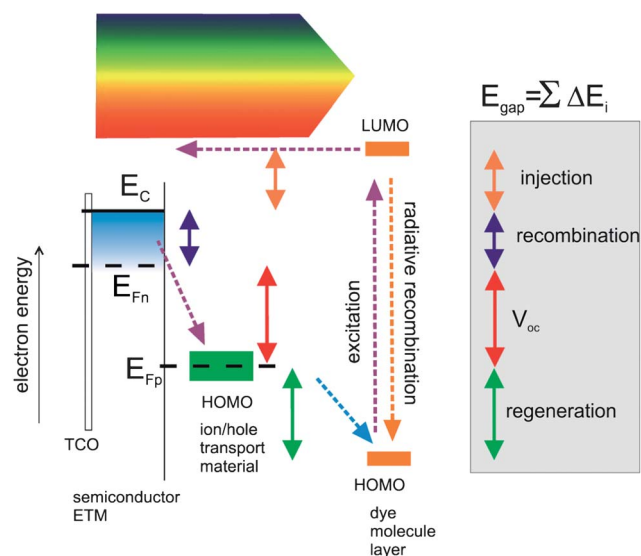


Fig. 10 Sketch of the energy diagram showing light absorption and charge transfer processes that occur in the DSC at open circuit. The origins of each of the energy losses in the cell, associated with injection, recombination and dye regeneration, are indicated, showing how the maximum potential, theoretically attainable by the solar cell, the gap energy of the dye, E_{gap} , is reduced to the actual open-circuit voltage V_{oc} . For clarity of presentation, the dye is not represented at the interface of the electron and hole transport materials, but separately on the right. E_C represents the conduction band bottom, E_{Fn} the electron quasi-Fermi level, E_{Fp} the hole quasi-Fermi level, and TCO the transparent conducting oxide acting as electron collector. Dashed arrows indicate the direction of the electron flow in the mentioned processes, while plain arrows indicate an energy difference.

$$(\Delta G^*) = (\Delta G^0 + \lambda)^2/4\lambda \quad (26)$$

Here λ is the reorganization energy (see Fig. 12). In molecular systems ΔG^0 is given by the difference in redox potential of D and A. While the difference in LUMO levels is often taken as such, only if the change in entropy can be neglected, $\Delta(\text{LUMO})$ will represent the change in free energy. λ depends on vibronic modes in the organic molecules. Fig. 12 shows the free energies of the states involved in the PIET process.

After initial PIET, the molecule with an extra electron (in higher vibronic level) can relax to its ground state and then to a Coulomb-bound state, due to the presence of the hole, or there can be electron transfer to another acceptor molecule if the intermolecular charge transfer rate is high (*i.e.*, λ for intermolecular electron transfer is small and the intermolecular electronic coupling for charge transfer is high), and then transition to the

state of the acceptor species. The electronic DOS in the semiconductor nanoparticle has an exponential shape, decreasing from the conduction band bottom towards the center of the gap. (c) The chemical capacitance of a number of DSCs with different dyes and electrolytes³² is plotted against V_F (the potential that describes the Fermi level position in the semiconductor). The horizontal shift is due to the difference in dye and supporting electrolyte between the different DSCs. Such electrochemical methods, that measure the chemical capacitance, provide a direct measurement of the electronic DOS in the semiconductor.

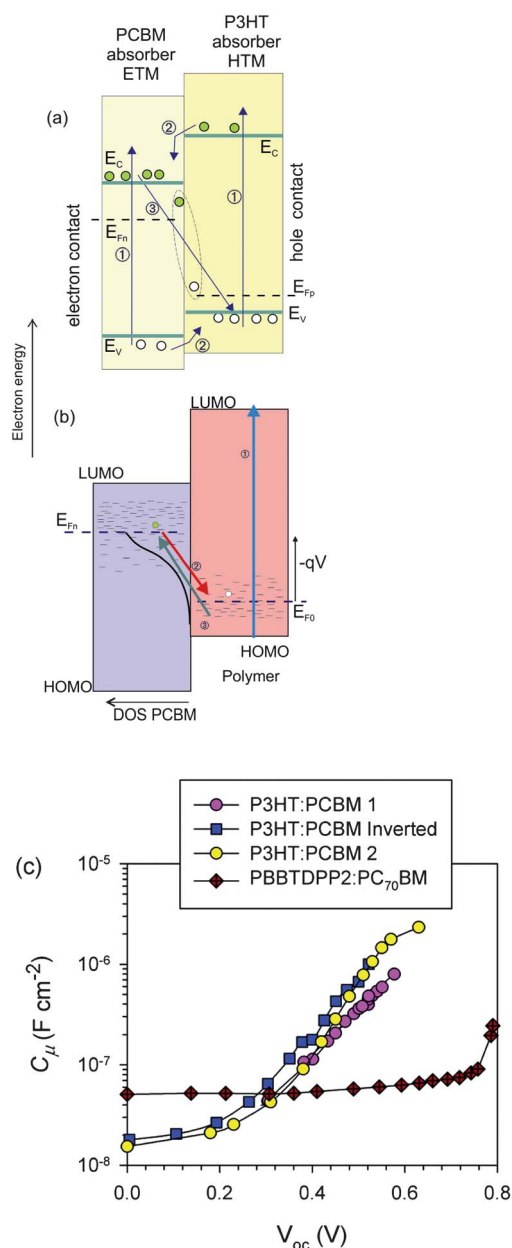


Fig. 11 (a) Energy diagram of an organic bulk heterojunction (BHJ) solar cell, consisting of a mixture of [6,6]-phenyl-C₆₁-butyric acid methyl ester (PCBM) and poly(3-hexylthiophene) (P3HT) and the following processes: (1) primary photoexcitation of the polymer or PCBM across the bandgap; (2) transfer of an electron or hole across the interface; and (3) recombination. A charge transfer exciton, formed by a bound electron-hole pair, of the carriers in different materials, is suggested. (b) As (a) but indicating the trap states in the bandgap of both materials, the equilibrium Fermi level (E_{F0}) and the electron quasi-Fermi level at 1 sun illumination (E_{Fn}). The arrows show the following processes. (1) Primary photoexcitation of the polymer across the bandgap, $h\nu = 1.85$ eV. (2) Recombination across the interface of an electron in PCBM close to the quasi-Fermi level with a hole close to the quasi-Fermi level in the polymer. (3) Photoexcitation of an electron close to the HOMO of the polymer, to a localized state close to the LUMO of the PCBM, $h\nu = 1.20$ eV. The density of states in PCBM is outlined. (c) The chemical capacitance of a number of BHJ solar cells, plotted against V_{oc} (measurement at open circuit at different illumination intensities).^{58–60} The measured capacitance corresponds to the DOS of PCBM that is outlined in (b).

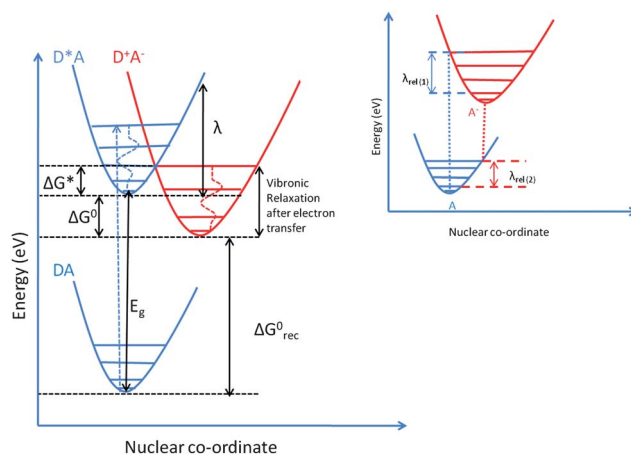


Fig. 12 Free energy diagrams for photo-induced electron transfer and vibronic relaxation after electron transfer. Dotted arrow shows the electronic transition from the ground state (DA) to the excited state (D*A). The minimum energy required to create (D*A) is given by E_g . Electron transfer is an activated process with the activation energy ΔG^* . ΔG^0 and ΔG_{rec}^0 are the changes in free energy of electron transfer and recombination, respectively. After electron transfer, the whole system relaxes to accommodate the extra charges in the donor and acceptor molecule (shown in parabola D*A⁻). The vibronic relaxation depends on the available vibronic modes in the system. The inset shows the relaxation energy for charge transfer, $\lambda_{rel}(1)$ and $\lambda_{rel}(2)$. The value, provided in the main text for hole relaxation, is $\lambda_{rel}(1)$, which we denote as λ_{rel} , because $\lambda_{rel}(1) \approx \lambda_{rel}(2)$. The reorganization energy is $\sim 2 \times$ relaxation energy.

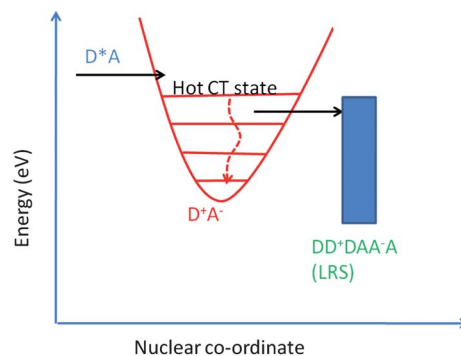


Fig. 13 The charge separated state of free electron and hole can be obtained *via* a hot charge transfer (CT) state, formed from an excited donor (D*)-acceptor (A) pair. The initial state (not shown) would be to the left of the diagram. LRS: Lattice Relaxed State. D*A⁻ stands for the lowest energy CT state, often denoted as CT₁.⁷¹

lattice-relaxed state, LRS polarons.³⁵ The polaron binding energy stabilizes the system, *via* rearrangement of the electron clouds around the separated charge, the electronic polarization, and *via* rearrangement of the nuclei around the charge, nuclear polarization.^{38–40}

In the case of disordered materials, this stabilization energy will be different for molecules at different sites due to differences in the local environment. If the Charge Transfer (CT) state has a lower energy than the LRS, the CT exciton will be separated by the excess energy stored in the vibronic levels (hot CT), as illustrated in Fig. 13. The carriers in the LRS determine the electronic free energy available in the system.

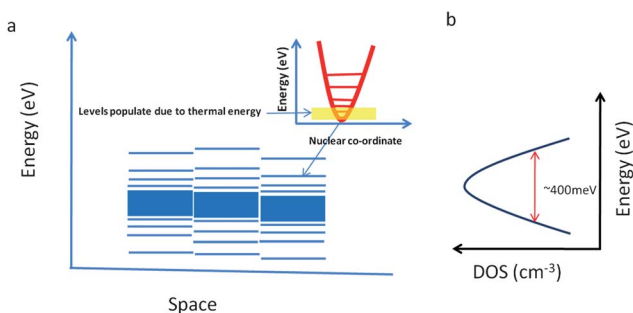


Fig. 14 Effect of static and dynamic (inset) disorder on the electronic energy levels of a system. (a) Electronic energy level distribution due to static disorder that can arise even from only loose packing of molecules in the crystal lattice.⁴⁴ Each horizontal bar represents the lower vibronic level of a molecule at a given site. The number of bars represents the number of molecules present in 2D space. However, due to thermal energy, higher vibronic levels can be populated. Inset: state diagram showing the different vibronic energy levels for a given state and (b) resulting broadening of states, due to both static and dynamic reasons.

In Fig. 14, the horizontal bars represent the fully relaxed molecules in their lattice position. Hence, the difference in polarization energy at different sites can be manifested as tail states.

The inset of Fig. 12 shows the relaxation energy $\lambda_{\text{rel}(1)}$ and $\lambda_{\text{rel}(2)}$ (λ_{rel}). This is the energy difference between a charged molecule in its original neutral geometry and the charged molecule in its relaxed geometry. The relaxation occurs *via* different vibronic modes, available to the molecule (see Fig. 12). As $\lambda_{\text{rel}(1)} \approx \lambda_{\text{rel}(2)}$, we denote the relaxation energy as λ_{rel} . Typical values for hole relaxation in thin films of stiff aromatic organic molecules are in the range of 70–150 meV.⁴¹ We can assume *at least* the same order for the relaxation energy for electrons, based on DFT calculations for organic molecules³⁹ and because of the more delocalized character of the LUMO than the HOMO (no experimental value of electron relaxation is available). Typical PIET involves relaxation of both the electron and the hole. The polymers that are used for OPV are significantly less stiff than say pentacene or a phthalocyanine, and we can thus expect the relevant λ_{rel} values for the hole (on the polymer) to be larger than those for which we quoted experimental results. Hence, the vibronic relaxation, associated with photo-induced charge transfer in OPV, is likely to be at least 150 and more likely close to 300 meV.

For efficient photocurrent production a few 100 meV (to overcome the Coulomb potential) have to be paid for efficient energy separation due to low dielectric constant of the organic material. The energy lost due to vibronic relaxation can be used to overcome the Coulomb potential and *may even be sufficient to overcome the Coulomb bound state; any additional energy that goes into vibronic relaxation is lost.*

From the above discussions we find that both reorganization energy and free energy change play a major role in the photocurrent production (first to produce the bound e–h pair from the exciton and then the separation of the e–h pair). We note that other mechanisms have been proposed for efficient photo-carrier generation at the O–O (donor–acceptor) interface and the reader is referred to the literature for these.⁴²

3.5 Tail states in an organic semiconductor

Another important aspect of heterogeneous solar cells, formed by low cost processes, is that the materials are often quite disordered, a feature already referred to a few times above. Besides the low mobilities that such disorder implies, which is beyond the scope of this paper, the distribution of states (tail states; see also Section 2.2) in the ETM and HTM plays a major role in determining the photovoltage and e–h recombination in both DSC and BHJ solar cells. Tail states, which are known to be present in amorphous materials, have also been identified in organic solids⁴³ including *highly crystalline* organic materials⁴⁴ (e.g., pentacene crystals), an observation that is especially relevant for small molecule-based organic cells. The reason is likely that the interactions between the components of the crystal are weaker than in inorganic non-molecular materials, leading to a more extensive thermal disorder (shallower potential well for minimum energy conformation). The origin of tail states is two-fold:

(a) static disorder as a result of loose crystal lattice and deformation of molecules.

(b) dynamic disorder due to the vibrational degrees of freedom of the molecules and the ensemble. Fig. 15 schematically describes the origin of tail states in organic solids.

Evidence for tail states. The edge broadening that is ascribed to tail states can be inferred from gas phase and solid state UPS spectroscopy. Ueno *et al.* described the effect of dynamic and static disorder on the UPS spectrum (see their figure from ref. 41, part of which is reproduced here as Fig. 15). They measured, by high resolution UPS, a hole relaxation energy in rigid aromatic organic materials of ~100 meV and a total broadening of ~200 meV.⁴¹ We can attribute the difference to static disorder. Another report on perylene and naphthalene tetracarboxylic di-anhydride (PTCDA and NTCDA) showed ~400–600 meV broadening of the HOMO level in the solid state.⁴⁵

Further evidence for tail states come from pinning of the Fermi level at several 100 meV above (below) the HOMO (LUMO) edge in many organic materials.^{43,46} Tengstedt *et al.*

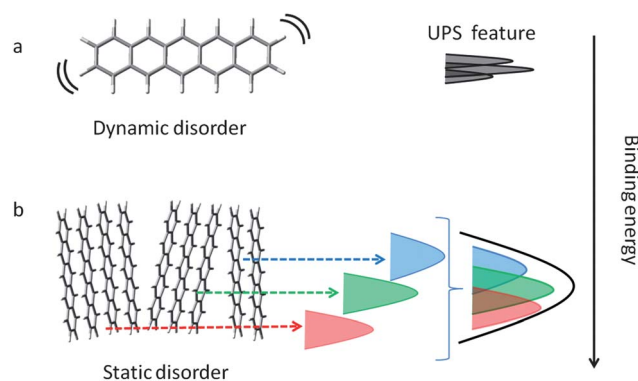


Fig. 15 Illustration of UPS-band shape and energy position for various molecular packing/orientations (based on UPS results of pentacene). (a) In the gas phase there is spread in the spectrum, due to the presence of different vibronic levels. This spread is dynamic and depends on temperature. (b) In the case of non-, micro- or nano-crystalline solids, the local energy levels differ with the surrounding structure (static disorder) (after Kera *et al.*; adapted with permission from ref. 41; © 2009 Elsevier).

observed such pinning and attributed it to E_F alignment with polaron levels of the organic semiconductor.⁴⁷ However, there is now ample evidence linking this phenomenon to the presence of tail states.^{43,48} Pinning of Fermi levels is also observed for organic semiconductors on other substrates, such as high work function metal oxides,⁴⁹ indicating that tail states are an inherent property of organic solids with some degree of disorder.

Understanding losses due to tail states. In the previous section we mentioned that the voltage loss in disordered inorganic cells, due to recombination *via* tail states, can be up to 0.3 V (in the case of a-Si). An important question is therefore whether losses are of the same order in disordered organics, and it has recently been suggested that this effect plays a dominant role in BHJ solar cells.^{50–52} In the case of a-Si recombination is dominated by trapped holes in the VB and the recombination, which is not an activated process, happens in the bulk of the material. For BHJ solar cells the recombination mechanism at V_{oc} is bimolecular in nature.^{53,54} The bimolecular recombination rate in a dielectric medium can be described by the Langevin rate:

$$k_L = q(\mu_n + \mu_p)/\epsilon\epsilon_0 \quad (27)$$

where μ_n and μ_p are the electron and hole mobilities, respectively. Experimentally determined recombination rates for BHJs are 2–3 orders magnitude smaller than the Langevin rates.^{53,54} These rates reflect a bimolecular process.^{53,54} One of the reasons for the lowered rate could be phase separation in the bulk, which creates domains for electron and hole transport so that recombination can only happen at the domains' interfaces. Another mechanism in series could be a Marcus type of recombination, where the non-geminate free electron and hole pair recombine to yield neutral molecules. In that case the observed recombination rate, k_{rec} , is given by

$$\frac{1}{k_{rec}} = \frac{1}{k_L} + \frac{1}{k_M} \quad (28)$$

where k_M is given by

$$k_M = k_0 e^{-(\Delta G_{rec}^0 + \lambda)^2 / 4\lambda k_B T} \quad (29)$$

This process is an activated one. The rate of recombination k_{rec} depends on the donor–acceptor coupling (k_0), reorganization energy (λ) and Gibbs free energy change on recombination ΔG_{rec}^0 . It is sometimes stated that recombination happens in the Marcus inverted region as the Gibbs free energy change in recombination is often higher than the reorganization energy of the event (*cf.* Fig. 12). In this case lower coupling and lower reorganization energy will result in a lowering of the recombination rate. However, it is experimentally observed that the output open-circuit voltage reached using a set of donor polymers with HOMO levels ranging from -4.6 eV down to -5.7 eV scales linearly with the blend effective bandgap interpreted as the $E_{(A)_{LUMO}} - E_{(D)_{HOMO}}$ energy difference.⁵⁵ If recombination occurs within the Marcus deep inverted region (k_M changes quadratically) the recombination flux is lowered for larger energy offsets. Under this assumption one might expect that V_{oc} would scale supralinearly with $E_{(A)_{LUMO}} - E_{(D)_{HOMO}}$. The recombination reduction is smoothed if charge transfer takes place around the

maximum of the Marcus expression implying larger reorganization energies. By using $\lambda \approx 1$ eV, simulations show that the open-circuit voltage linearity with effective bandgap is preserved.⁵⁰

The role of the coupling constant (k_0) has been discussed in various articles.^{56,57} It appears that structural disorder at the interface as well as relative orientation (rotational disorder) of D and A with respect to each other may also affect the coupling constant⁵⁶ which in turn affects the kinetics of recombination (as well as charge separation). The typical recombination rates for these materials are 10^{-12} to 10^{-14} $\text{cm}^{-3} \text{s}^{-1}$.

Quantifying tail states. In a typical organic material, the density of states (DOS) in HOMO or LUMO level is of the order of $\sim 10^{20} \text{cm}^{-3}$. Under normal insolation the photogenerated carrier density for a material with an optical bandgap of ~ 1.85 eV is between 10^{16} and 10^{17}cm^{-3} ,^{53,58} depending on various material parameters, especially the recombination rates. As the carriers in organic semiconductors move *via* hopping (*i.e.*, slow and thus can fall into traps), photo-generated carriers always populate these tail states.⁵⁰ Recombination of electrons and holes occurs *via* these tail states, and the rate of recombination is such that, at one sun illumination, these tail states are not filled completely. In fact the carriers accumulate in broad bands of localized states, as suggested in a scheme for the BHJ in Fig. 11(b). Measurements of the DOS by the chemical capacitance, as indicated before in eqn (25), are shown in Fig. 11(c) for P3HT:PCBM in regular and inverted configuration^{58,59} and for PBBTDP2:PC₇₀BM.⁶⁰ The DOS in the PCBM has an exponential shape that sometimes could be interpreted as a Gaussian as well. Measurement of the DOS above voltage higher than V_{oc} at one sun has so far been complicated by the appearance of negative capacitance and so the full shape of the DOS is not known. The quasi-Fermi level position is determined by the free-carrier concentration, which in turn depends on the balance between the rates of photo-generation and recombination. The carrier density is modulated by the shape and energy position of available electronic states, which in real devices exhibit featured distributions entering the bandgap. Crystallization or molecule aggregation changes the actual DOS within the bandgap and are therefore key aspects for determining electronics aspects in the solar cell after blend formation. The capacitance measurements are a direct technique able to extract a detailed view on absolute energy and state distributions using complete devices. As shown in Fig. 11(c) capacitance analysis shows the occupation of acceptor states (fullerene DOS). The use of different polymers produces a shift in the capacitance onset related to the position of the HOMO acceptor. Such a position is known to depend on blend processing conditions and final morphology, and can be considered as a reference for the device energetics. Moreover, it has been shown that for the P3HT:PCBM system, the loss due to tail states could be of the order of 200 mV. As the separation of quasi-Fermi levels is dictated by recombination and these tail states, any lowering in recombination rate (by smart design of molecules) would be helpful in increasing the V_{oc} .⁵⁰

Modeling and analyzing tail states. Rau and Werner⁶¹ analyzed the effect of tail states in a single absorber system, taking into account their influence on spatial distribution of the bandgap. In

BHJ cells, one can also apply the same logic, where the distribution in bandgap is linked to the tails in HOMO energy of the donor and in the LUMO energy of the acceptor.⁵⁰ If a Gaussian distribution is considered for the electronic states, the photo-generated carriers, which are initially distributed along density-of-states shape, thermalize in the Gaussian tail following a Boltzmann statistics in the case of low occupancy with an average, equilibration energy $\sigma_n/k_B T$ below E_{LUMO} . Such an energy signals the mean energy level of the charge carriers and is located above the concentration-dependent Fermi energy.⁶² A straightforward calculation allows determining the Fermi level positions⁶³ from which an expression for V_{oc} can be readily given:⁶⁴

$$qV_{\text{oc}} = E_g - \frac{\sigma_n^2 + \sigma_p^2}{2k_B T} - k_B T \ln \left(\frac{N_n N_p}{np} \right) \quad (30)$$

Here E_g is the effective bandgap, *i.e.*, the difference between the transport levels for holes (HOMO of donor) and electrons (LUMO of acceptor). The second summand contains the term related to the electron and hole equilibration energies, which establish an upper limit to the achievable photovoltage, and might be interpreted in terms of a reduction in the effective bandgap E_g (~ 400 mV for $\sigma \approx 100$ meV at room temperature). It appears as a distinctive feature of organic disordered compounds related to the Gaussian DOS occupancy.

Reducing tail state density. A possible way of negating the effect of tail states could be by permanently filling the tail states by dopant molecules. In the case of a-Si it has been found that doping indeed fills tail states. A recent study by Deschler *et al.*⁶⁵ reveals that p-doping of an organic polymer (with organic dopant) fills the tail states in the HOMO manifold and affects the optical, charge transfer and recombination properties of the system. The filling of tail states also improves the charge transport, as filled states do not trap carriers and consequently do not affect transport.^{66,67}

We note that in the case of a DSC (with TiO_2 as n-type semiconductor) the tail states, though present,⁶⁸ dynamically fill after photo-induced charge transfer from the dye. Hence the electron quasi-Fermi level can be close to the CB of TiO_2 . The same process does not take place in the organics used for OPV, because recombination from tail states is likely to be much faster. This can be due to the higher degree of local disorder in the materials used in a BHJ OPV than in a DSC (an idea that can be tested experimentally by comparing data for nano-crystalline organics with those of the common BHJ cells).

4. Fill factor and disorder

From eqn (16), we can infer that FF depends on V_{oc} (which in turn depends on the bandgap of the material) and diode quality factor n . Due to the presence of multiple ways of recombination in a disordered material, n is higher than that of a crystalline material. Table 1 summarizes the values for best cells in different categories. Though empirical, a trend arises from the compiled data. For perfect crystalline cells, the value of FF is 80–85% while for organic based cells it is 65–70%, with intermediate values for disordered inorganic ones, though the values of V_{oc} are comparable in many cases. Fig. 16 describes the distribution of FF

Table 1 Fill Factor (FF) values for best cells in different categories. Data taken from ref. 5, 12 and 72

Cell type	Bandgap (eV)	V_{oc} (V)	FF (%)
Si	1.12	0.71	82.8
GaAs	1.42	1.11	85.9
InP	1.28	0.88	85.4
CIGS	1.15	0.71	79.2
CdTe	1.45	0.84	75.5
a-Si	1.73	0.89	67
DSC (black dye)	1.3	0.74	68
DSC (N719)	1.6	0.82	74
DSC (YD2-o-c8 + Y123) ^a	1.7	0.93	74
Organic Polymer (Konarka)	1.65	0.82	70.2
Organic Small Molecule (Mitsubishi)	1.66	0.90	66.1

^a ref.72, in-house measurement, see also ref. 5.

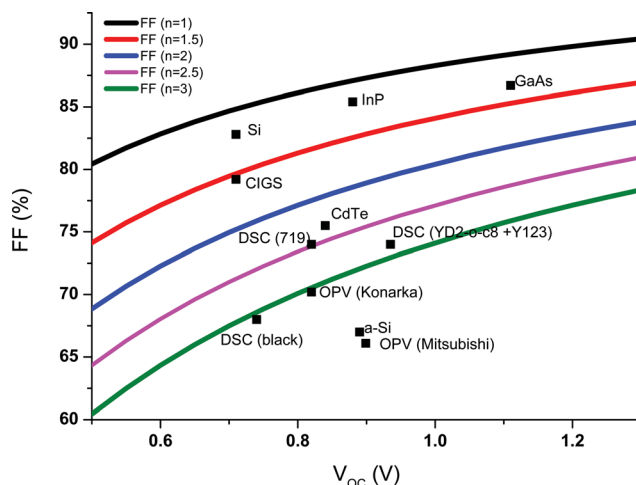


Fig. 16 Fill Factors (FF) of best laboratory cells (as of Dec. 2011) of different categories. The solid lines represent the expected FF value for a given value of n . The disorder impacts the FF value of the cell due to higher number of recombination mechanism. CIGS stands for Cu (In,Ga)Se₂; OPV stands for Organic PhotoVoltaic cell, with the laboratory that made the cell in parentheses as, unfortunately, the actual material compositions are not always released; DSC indicates Dye sensitized solar cell with the dye used in parentheses.

values over different type of cells. We can see that a good amount of extra loss happens in organic based cells compared to crystalline cells.

5. Projected efficiencies

From the discussions presented here we can infer that in addition to the fundamental losses, which are applicable to 1st generation solar cells, DSCs and OPVs have several other loss mechanisms, namely, vibronic loss (dynamic disorder), dielectric loss and tail state loss (static disorder). Though these losses are interdependent, if not addressed properly, their combined effect will reduce the maximum achievable efficiency significantly. We can also include other loss mechanisms like EQE loss due to the optical absorption spectrum of the organic absorber as the optical absorption is primarily molecular in nature and the transition dipole varies with electronic levels. Because of limits on how

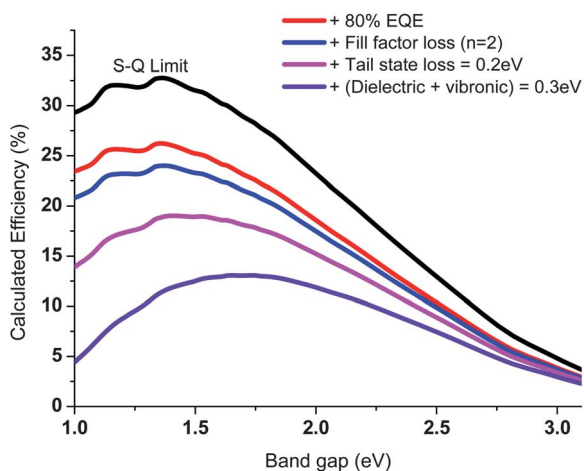


Fig. 17 Calculated efficiency of OPV, based on S-Q limit, with different loss mechanisms added, as a function of absorption edge energy. As discussed in the text, vibronic loss can compensate for dielectric loss. Clearly any improvement beyond the assumptions made here, *e.g.*, >80% EQE, $n < 2$, decreased density of tail state, higher effective dielectric constant and decreased vibronic loss, will improve the estimates, *i.e.*, push the curves towards higher likely efficiencies and lower optimal bandgaps.

thick the films can be made, the EQEs of organic cells are smaller than inorganic ones and <100%. Fig. 7 gives an example of such a case. We can make an educated guess for EQE of OPV cells as 80%. Due to the presence of disorder induced defect centers, there can be more than one type of recombination mechanism. From eqn (16), we see that FF is dependent on the ideality factor n , which in turn depends on the importance of various recombination processes. Hence more than one type of recombination can reduce the FF. However, we cannot derive a clear lower or upper limit of the diode ideality factor for OPVs. We will take, $n = 2$, for the present purpose of estimating OPV efficiency limits, based on the best cells presently reported in the literature. We note here that the FF loss also depends on cell processing. Fig. 17 gives an estimate of efficiency of OPVs with different loss mechanism for a given bandgap absorber. Here we note that V_{oc} of the organic based cell can be related to optical gap of the absorber by taking into account the driving force for charge separation and vibronic loss after charge separation.

With all the additional losses, the focus on ~ 1.4 eV absorbers, based on pure SQ analysis, central to much PV development, would appear to be somewhat misguided for molecular cells.

6. Challenge and future of solar cells based on organic materials

One can get a sense of the development profile for these kinds of cells over the years by looking at the periodically updated “Best Research-Cell Efficiency” plot on the National Renewable Energy Laboratory (NREL) website (<http://www.nrel.gov/ncpv/>). In a previous paper¹² we also provide information (which we update on our website <http://www.weizmann.ac.il/materials/Cahen/links>) about the performance of various solar cells. The trend shows that over the past few years organic molecule-based cells have improved significantly. However, organic materials are often unstable in the presence of light and air. Thus, the stability

issue associated with OPVs has to be addressed for commercial success of these cells. A small percentage of degradation in one cell that is part of a commercial module can bring down the efficiency of the whole module. Encapsulation of these cells can solve stability issues, due to ambient atmosphere and, indeed, there is no commercial solar cell today that is not encapsulated. However, the requirements for organics are likely to be more strict and the material and technique should be compatible with contacts and photo-active materials. This extra caution in encapsulation may increase the cost of production. There is hope in this regard from the development history of Organic Light Emitting Devices (OLEDs). During the early days of development, OLEDs also faced stability issues from the ambient. Now OLEDs show up to 10^5 h operational lifetime, making them commercially viable. Furthermore, the excellent lifetime of certain organics in paints, especially for automobiles, is often cited to show that the problem is not an intrinsic one for cheap, mass-manufacturable materials.

7. Summary

After decades of research and development, solar cells that are based on disordered material(s) lag behind their more crystalline counterparts in efficiency as well as in commercialization. Two types of disorder are involved, which are static and dynamic in nature. The former is present even without any energy input into the system, while the latter comes about with such an energy input, most commonly as vibrations and rotations for molecules, which, for non-molecular systems, are expressed as phonon modes. The basic physico-chemical limitations in terms of the photovoltaic effect, arising from their disorder, are reflected in the overall performance of these cells. Disorder affects the electronic energies available (tail states). These states can dominate recombination, which can be non-geminate. Energy disorder in the electron (or hole) transport material also increases the energy differences between the band edges or their molecular equivalents and the quasi-Fermi levels, which implies that we pay a price in terms of photovoltage.

In the case of organic molecular materials the energies involved in vibronic modes lead to an additional loss because of relaxation of photo-generated carriers. However, this same vibronic loss may help to overcome Coulomb attraction in low dielectric materials. One way to mitigate the effect of tail states, which seems to be inherent in low-cost materials on available photovoltage, is to fill these states by chemical doping. To minimize the vibronic loss, new material design is required, where, though, care should be taken, so that the charge separation at the interface is not affected.

In case the absorber and transport materials are separated (*e.g.*, in the DSC) this can help to optimize materials separately, but carries a price in terms of increased probability for non-radiative recombination, as reflected experimentally in very low electroluminescence, and in low photovoltaic efficiency.

Acknowledgements

We thank Prof. K. L. Narasimhan (Tata Institute of Fundamental Research, Mumbai, India) and Prof. N. Ueno (Chiba Univ., Japan) for very valuable discussions. We are grateful to

the US–Israel Binational Science Foundation (AK, DC), the Israel Ministry of Science and Technology, the Britain-Israel Research and Academic Partnership, BIRAX, the Monroe and Majorie Burk Fund for Alternative Energy studies (all to DC), the Nancy and Stephen Grand Center for Sensors and Security (DC & PKN), the European Union (ORION CP-IP 229036-2), the Ministerio de Ciencia e Innovación (MICINN) of Spain (HOPE CSD2007-00007 (Consolider-Ingenio 2010)), and Generalitat Valenciana (PROMETEO/2009/058) (all to JB) for partial support. DC holds the Rowland and Sylvia Schaefer chair in Energy Research.

References

- 1 B. O'Regan and M. Grätzel, *Nature*, 1991, **353**, 737–740.
- 2 S. H. Park, A. Roy, S. Beaupre, S. Cho, N. Coates, J. S. Moon, D. Moses, M. Leclerc, K. Lee and A. J. Heeger, *Nat. Photonics*, 2009, **3**, 297–302.
- 3 W. Shockley and H. J. Queisser, *J. Appl. Phys.*, 1961, **32**, 510–519.
- 4 J. Zhao, A. Wang, M. A. Green and F. Ferrazza, *Appl. Phys. Lett.*, 1998, **73**, 1991.
- 5 M. A. Green, K. Emery, Y. Hishikawa, W. Warta and E. D. Dunlop, *Prog. Photovoltaics Res. Appl.*, 2012, **20**, 12–20.
- 6 J. F. Guillemoles, in *Fundamentals of Materials for Energy and Environmental Sustainability*, Cambridge University Press, New York, 2011, p. 238.
- 7 G. P. Smestad, F. C. Krebs, C. M. Lampert, C. G. Granqvist, K. Chopra, X. Mathew and H. Takakura, *Sol. Energy Mater. Sol. Cells*, 2008, **92**, 371–373.
- 8 (a) D. Cahen, G. Hodes, M. Grätzel, J. F. Guillemoles and I. Riess, *J. Phys. Chem. B*, 2000, **104**, 2053–2059; (b) J. Bisquert, D. Cahen, G. Hodes, S. Rühle and A. Zaban, *J. Phys. Chem. B*, 2004, **108**, 8106–8118.
- 9 K. Walzer, B. Maennig, M. Pfeiffer and K. Leo, *Chem. Rev.*, 2007, **107**, 1233–1271.
- 10 M. A. Green, *Sol. Cells*, 1982, **7**, 337–340.
- 11 J. Bisquert and I. Mora-Seró, *J. Phys. Chem. Lett.*, 2010, **1**, 450–456.
- 12 P. K. Nayak, J. Bisquert and D. Cahen, *Adv. Mater.*, 2011, **23**, 2870–2876.
- 13 Q. Yu, S. Liu, M. Zhang, N. Cai, Y. Wang and P. Wang, *J. Phys. Chem. C*, 2009, **113**, 14559–14566.
- 14 Y. Liang, Z. Xu, J. Xia, S. Tsai, Y. Wu, G. Li, C. Ray and L. Yu, *Adv. Mater.*, 2010, **22**, E135–E138.
- 15 R. T. Ross, *J. Chem. Phys.*, 1967, **46**, 4590.
- 16 U. Rau, *Phys. Rev. B: Condens. Matter Mater. Phys.*, 2007, **76**, 085303.
- 17 T. Kirchartz and U. Rau, *Phys. Status Solidi A*, 2008, **205**, 2737–2751.
- 18 O. D. Miller, E. Yablonovitch, and S. R. Kurtz, arXiv:1106.1603, 2011.
- 19 K. Vandewal, K. Tvingstedt, A. Gadisa, O. Inganäs and J. V. Manca, *Nat. Mater.*, 2009, **8**, 904–909.
- 20 M. A. Green, *Prog. Photovoltaics Res. Appl.*, 2011, DOI: 10.1002/pip.1147.
- 21 R. S. Crandall, *Phys. Rev. Lett.*, 1980, **44**, 749.
- 22 T. Tiedje, *Appl. Phys. Lett.*, 1982, **40**, 627.
- 23 L. M. Peter, *Phys. Chem. Chem. Phys.*, 2007, **9**, 2630.
- 24 C. J. Brabec, N. S. Sariciftci and J. C. Hummelen, *et al.*, *Adv. Funct. Mater.*, 2001, **11**, 15–26.
- 25 B. Valeur, *Molecular Fluorescence: Principles and Applications*, Wiley-VCH, 2001.
- 26 In the static (or frozen orbital) approach the orbitals are the same for ions and neutral molecules. This is known as Koopmans theorem. In this approximation the vertical ionization energy (which is what is expressed in the so-called energy or band diagrams that use 1 electron energies, cf. Fig. 3 and 8–11) of the molecule is equal to the negative of the Highest Occupied Molecular Orbital (HOMO) energy. Similarly the vertical electron affinity (EA) will then equal the energy of the LUMO. In this approach, electron–electron correlation is neglected and the approach is valid for isolated molecules. The singlet excited state of a molecule is formed if one electron from the HOMO is promoted to the LUMO. This approximation can be extended to solid molecular systems, as long as the interactions among the constituent molecules can be neglected.
- 27 P. K. Nayak and N. Periasamy, *Org. Electron.*, 2009, **10**, 1396–1400.
- 28 J. Bisquert and G. Garcia-Belmonte, *J. Phys. Chem. Lett.*, 2011, **2**, 1950–1964.
- 29 M. Riede, T. Mueller, W. Tress, R. Schueppel and K. Leo, *Nanotechnology*, 2008, **19**, 424001.
- 30 S. Ardo and G. J. Meyer, *Chem. Soc. Rev.*, 2009, **38**, 115.
- 31 J. Bisquert, F. Fabregat-Santiago, I. Mora-Seró, G. Garcia-Belmonte and S. Giménez, *J. Phys. Chem. C*, 2009, **113**, 17278–17290.
- 32 F. Fabregat-Santiago, G. Garcia-Belmonte, I. Mora-Seró and J. Bisquert, *Phys. Chem. Chem. Phys.*, 2011, **13**, 9083–9118.
- 33 H. Reiss, *J. Phys. Chem.*, 1985, **89**, 3783–3791.
- 34 Q. Wang, S. Ito, M. Grätzel, F. Fabregat-Santiago, I. Mora-Seró, J. Bisquert, T. Bessho and H. Imai, *J. Phys. Chem. B*, 2006, **110**, 25210–25221.
- 35 T. M. Clarke and J. R. Durrant, *Chem. Rev.*, 2010, **110**, 6736–6767.
- 36 M. M. Wienk, J. M. Kroon, W. J. H. Verhees, J. Knol, J. C. Hummelen, P. A. van Hal and R. A. J. Janssen, *Angew. Chem.*, 2003, **115**, 3493–3497.
- 37 R. A. Marcus, *Rev. Mod. Phys.*, 1993, **65**, 599.
- 38 In the cases of molecules, the latter can be divided into molecular geometric relaxation and lattice geometry relaxation. The time scale of lattice relaxation is too slow to be detected by UPS measurements. However, the charge–vibronic coupling (due to relaxation of the molecular geometry) can be probed by UPS. The contribution due to nuclear relaxation of near by molecules (lattice relaxation in the case of crystals) to polaron binding energy is often negligible compared to the electronic contribution. For example, for anthracene the calculated value is ~15 meV (ref. 39).
- 39 V. Coropceanu, J. Cornil, D. A. da Silva Filho, Y. Olivier, R. Silbey and J.-L. Brédas, *Chem. Rev.*, 2007, **107**, 926–952.
- 40 Here we note that band transport, though possible, is expected to be significant only in very high quality crystals at low temperatures, while here we are concerned with what are at least partially disordered materials at room temperature.
- 41 S. Kera, H. Yamane and N. Ueno, *Prog. Surf. Sci.*, 2009, **84**, 135–154.
- 42 V. I. Arkhipov, P. Heremans and H. Bässler, *Appl. Phys. Lett.*, 2003, **82**, 4605.
- 43 J. Hwang, A. Wan and A. Kahn, *Mater. Sci. Eng., R*, 2009, **64**, 1–31.
- 44 W. L. Kalb, S. Haas, C. Krellner, T. Mathis and B. Batlogg, *Phys. Rev. B: Condens. Matter Mater. Phys.*, 2010, **81**, 155315.
- 45 J. Sauther, J. Wüsten, S. Lach and C. Ziegler, *Phys. Status Solidi C*, 2007, **4**, 1844–1851.
- 46 J. Hwang, E.-G. Kim, J. Liu, J.-L. Brédas, A. Duggal and A. Kahn, *J. Phys. Chem. C*, 2006, **111**, 1378–1384.
- 47 C. Tengstedt, W. Osikowicz, W. R. Salaneck, I. D. Parker, C.-H. Hsu and M. Fahlman, *Appl. Phys. Lett.*, 2006, **88**, 053502.
- 48 W. L. Kalb, S. Haas, C. Krellner, T. Mathis and B. Batlogg, *Phys. Rev. B: Condens. Matter Mater. Phys.*, 2010, **81**, 155315.
- 49 J. Meyer, K. Zilberberg, T. Riedl and A. Kahn, *J. Appl. Phys.*, 2011, **110**, 033710.
- 50 G. Garcia-Belmonte and J. Bisquert, *Appl. Phys. Lett.*, 2010, **96**, 113301.
- 51 J. C. Blakesley and D. Neher, *Phys. Rev. B: Condens. Matter Mater. Phys.*, 2011, **84**, 075210.
- 52 T. Kirchartz, B. E. Pieters, J. Kirkpatrick, U. Rau and J. Nelson, *Phys. Rev. B: Condens. Matter Mater. Phys.*, 2011, **83**, 115209.
- 53 C. G. Shuttle, B. O'Regan, A. M. Ballantyne, J. Nelson, D. D. C. Bradley and J. R. Durrant, *Phys. Rev. B: Condens. Matter Mater. Phys.*, 2008, **78**, 113201.
- 54 S. R. Cowan, A. Roy and A. J. Heeger, *Phys. Rev. B: Condens. Matter Mater. Phys.*, 2010, **82**, 245207.
- 55 M. C. Scharber, D. Mühlbacher, M. Koppe, P. Denk, C. Waldauf, A. J. Heeger and C. J. Brabec, *Adv. Mater.*, 2006, **18**, 789–794.
- 56 V. Lemaire, M. Steel, D. Beljonne, J.-L. Brédas and J. Cornil, *J. Am. Chem. Soc.*, 2005, **127**, 6077–6086.
- 57 C. W. Schlenker and M. E. Thompson, *Chem. Commun.*, 2011.
- 58 G. Garcia-Belmonte, P. P. Boix, J. Bisquert, M. Lenes, H. J. Bolink, A. La Rosa, S. Filippone and N. Martín, *J. Phys. Chem. Lett.*, 2010, **1**, 2566–2571.
- 59 P. P. Boix, J. Ajuria, I. Etxebarria, R. Pacios, G. Garcia-Belmonte and J. Bisquert, *J. Phys. Chem. Lett.*, 2011, **2**, 407–411.
- 60 P. P. Boix, M. M. Wienk, R. A. J. Janssen and G. Garcia-Belmonte, *J. Phys. Chem. C*, 2011, **115**, 15075–15080.

-
- 61 U. Rau and J. H. Werner, *Appl. Phys. Lett.*, 2004, **84**, 3735.
- 62 H. Bässler, *Phys. Status Solidi B*, 1993, **175**, 15–56.
- 63 S. D. Baranovskii, I. P. Zvyagin, H. Cordes, S. Yamasaki and P. Thomas, *Phys. Status Solidi B*, 2002, **230**, 281–288.
- 64 G. Garcia-Belmonte, *Sol. Energy Mater. Sol. Cells*, 2010.
- 65 F. Deschler, E. Da Como, T. Limmer, R. Tautz, T. Godde, M. Bayer, E. von Hauff, S. Yilmaz, S. Allard and U. Scherf, *et al.*, *Phys. Rev. Lett.*, 2011, **107**, 127402.
- 66 Y. Qi, T. Sajoto, M. Kröger, A. M. Kandabarow, W. Park, S. Barlow, E.-G. Kim, L. Wielunski, L. C. Feldman, R. A. Bartynski, J.-L. Brédas, S. R. Marder and A. Kahn, *Chem. Mater.*, 2009, **22**, 524–531.
- 67 Y. Zhang, B. de Boer and P. W. M. Blom, *Phys. Rev. B: Condens. Matter Mater. Phys.*, 2010, **81**, 085201.
- 68 I. Abayev, A. Zaban, V. G. Kytin, A. A. Danilin, G. Garcia-Belmonte and J. Bisquert, *J. Solid State Electrochem.*, 2007, **11**, 647–653.
- 69 M. A. Green, K. Emery, Y. Hishikawa and W. Warta, *Prog. Photovoltaics Res. Appl.*, 2010, **18**, 346–352.
- 70 H. Gerischer, *Electrochim. Acta*, 1990, **35**, 1677–1699.
- 71 X. Zhu and A. Kahn, *MRS Bull.*, 2010, **35**, 443–448.
- 72 A. Yella, H. -W. Lee, H. N. Tsao, C. Yi, A. K. Chandiran, M. D. K. Nazeeruddin, E. W. -G. Diau, C. -Y. Yeh, S. M. Zakeeruddin and M. Grätzel, *Science*, 2011, **334**, 629–634.